Supplementary Materials

Synthesis of thiophene-fused siloles through rhodium-catalyzed *trans*-bis-silylation

Akinobu Naka,[1,*] Maho Inoue,[1] Haruna Kawabe,[1] and Hisayoshi Kobayashi[2,*]

[1] Department of Life Science, Kurashiki University of Science and the Arts, Nishinoura, Tsurajima-cho, Kurashiki, Okayama 712-8505, Japan

[2] Professor Emeritus Kyoto Institute of Technology, Matsugasaki, Kyoto 606-8585, Japan

E-mail addresses: anaka@chem.kusa.ac.jp (A. Naka), hisabbit@yahoo.co.jp (H. Kobayashi)

Contents

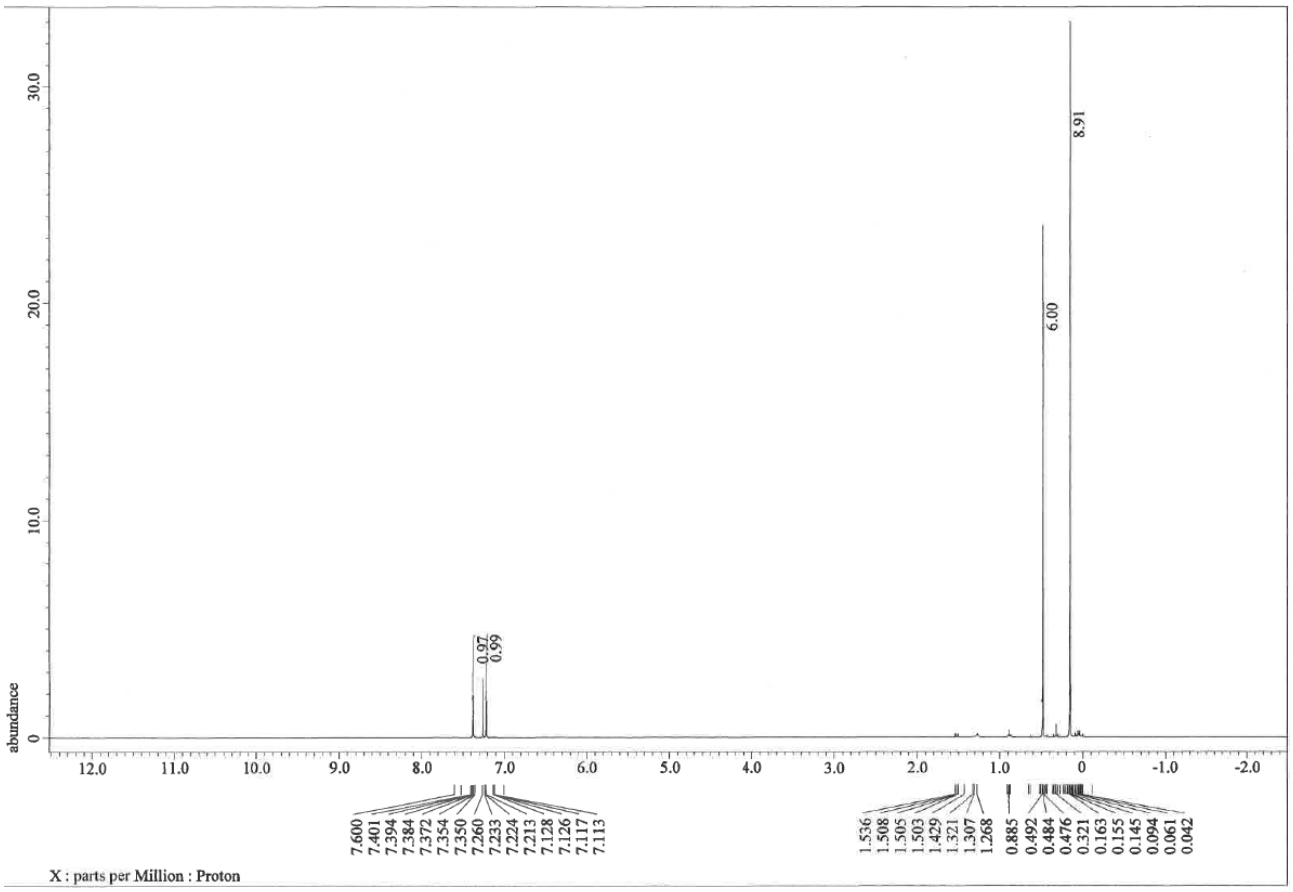

Figure S1. ^{1}H NMR spectrum of 3-iodo-2-(1,1,2,2,2-pentamethyldisilanyl)thiophene in $CDCl_3$.

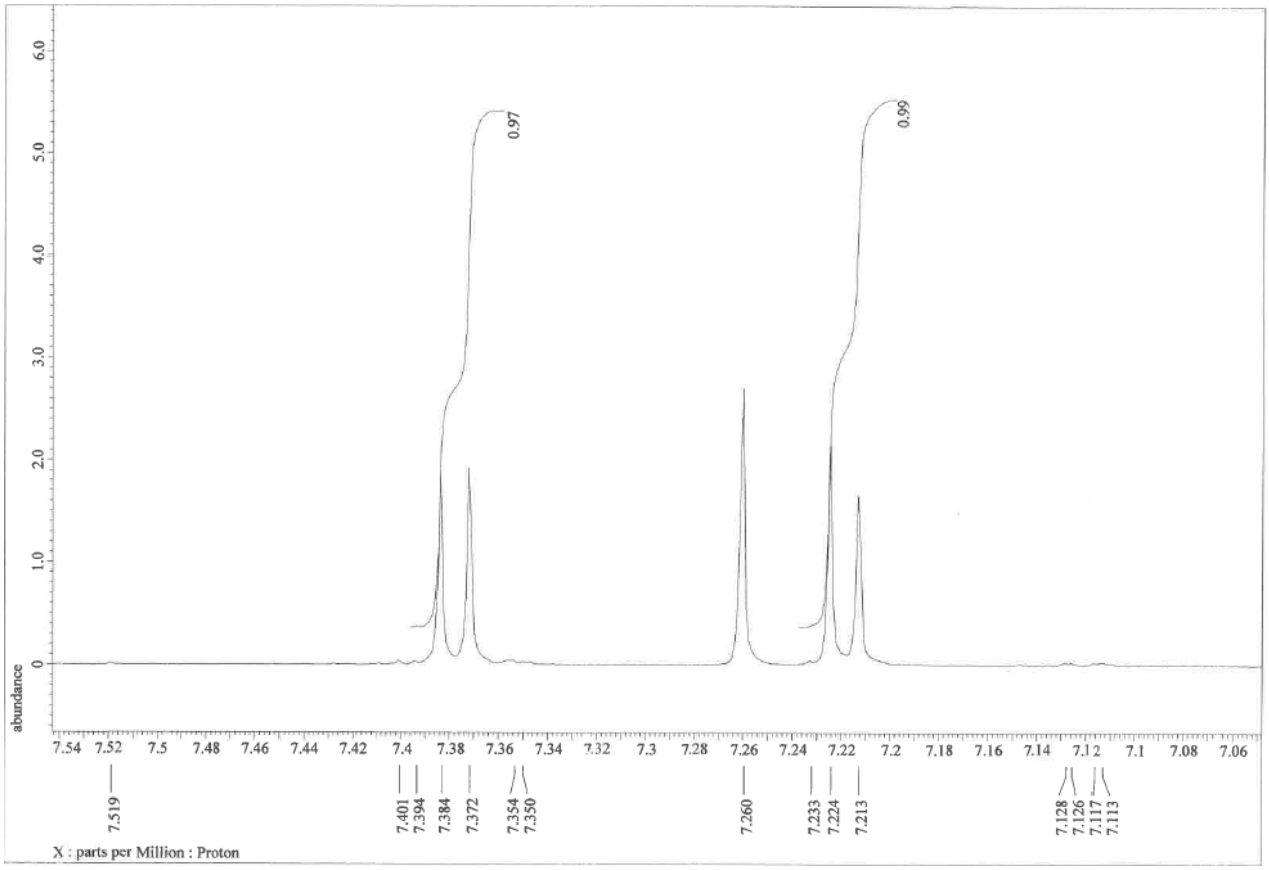

Figure S2. Enlarged view of the aromatic region for 3-iodo-2-(1,1,2,2,2-pentamethyldisilanyl)thiophene in $CDCl_3$.

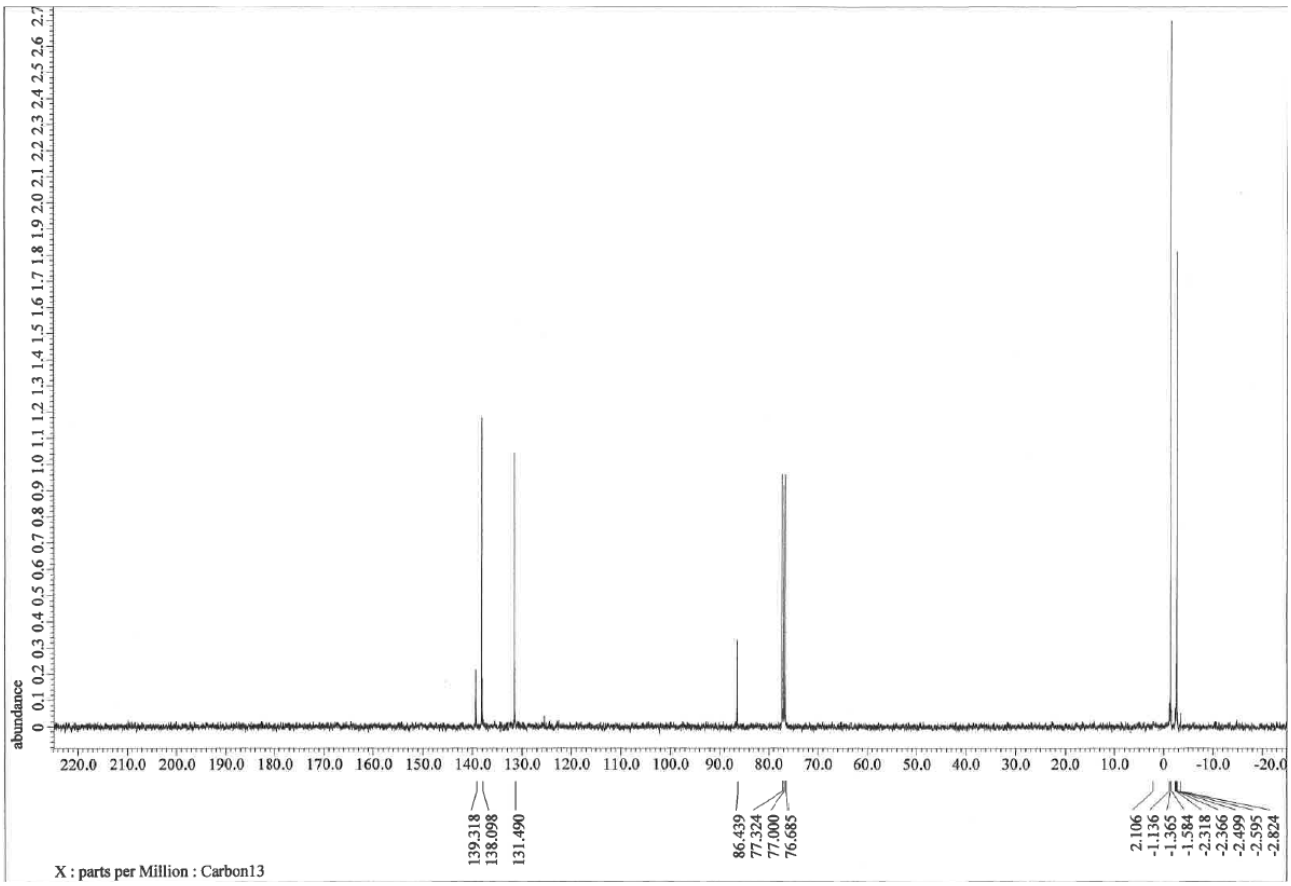

Figure S3. ^{13}C NMR spectrum of 3-iodo-2-(1,1,2,2,2-pentamethyldisilanyl)thiophene in $CDCl_3$.

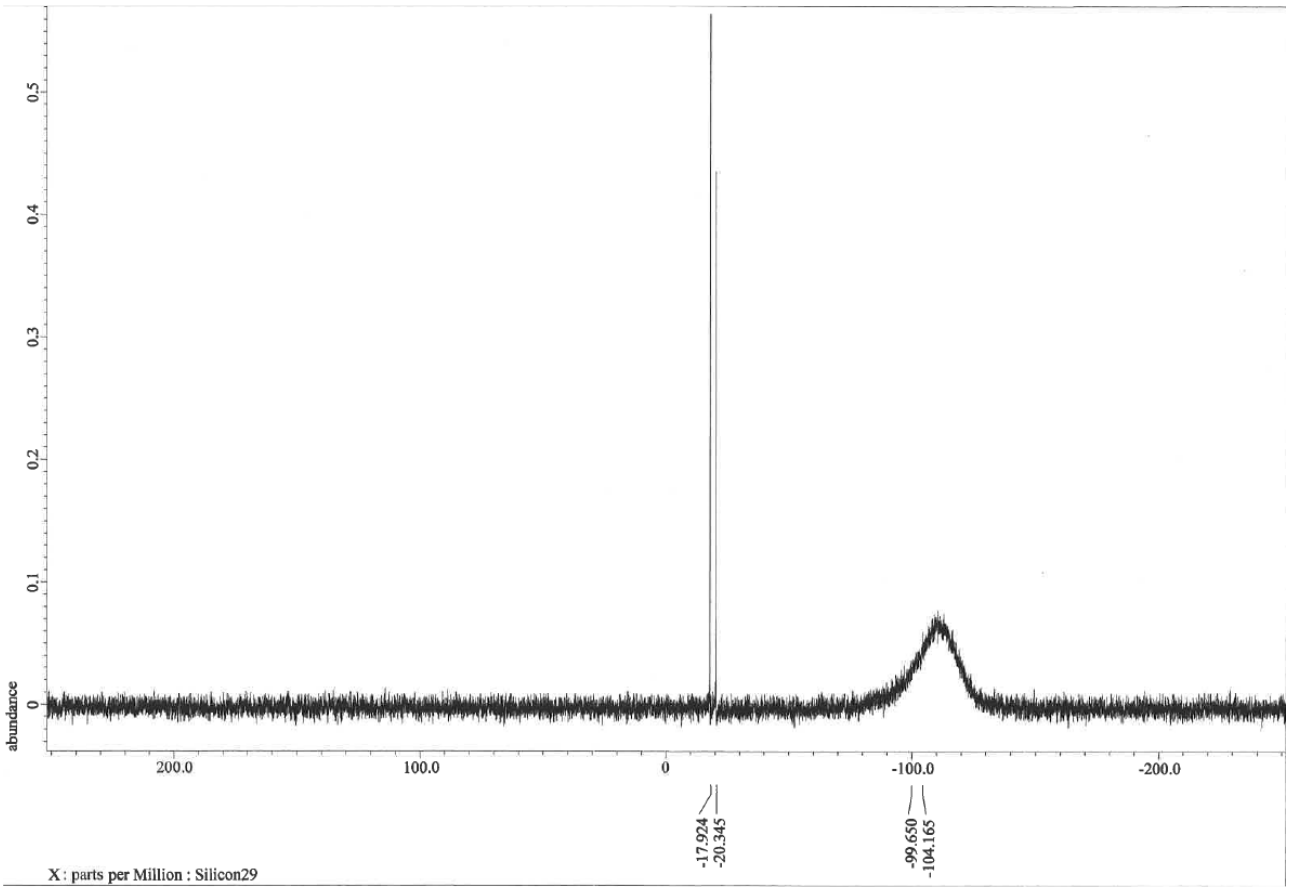

Figure S4. ^{29}Si NMR spectrum of 3-iodo-2-(1,1,2,2,2-pentamethyldisilanyl)thiophene in $CDCl_3$.

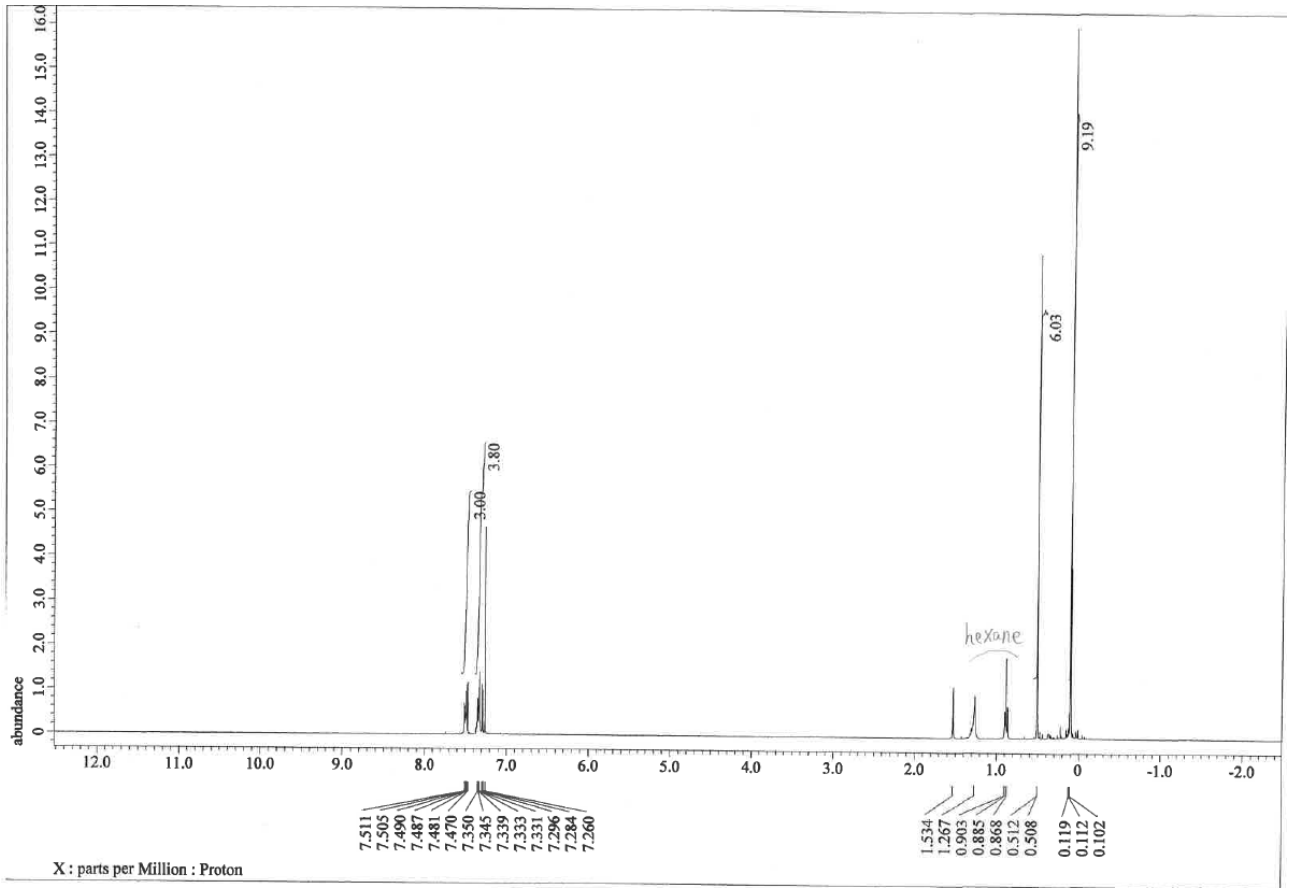

Figure S5. ^{1}H NMR spectrum of **1a** in $CDCl_3$.

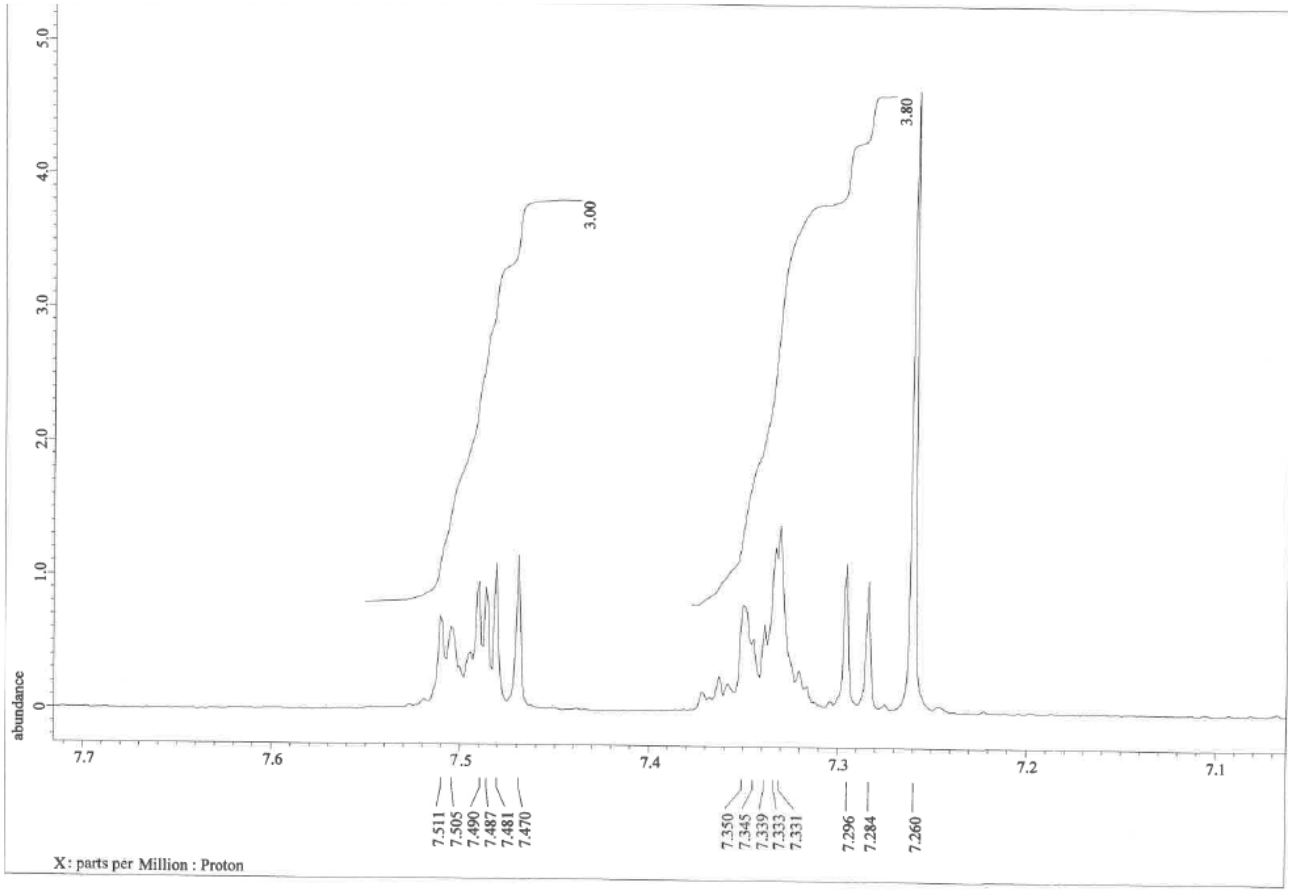

Figure S6. Enlarged view of the aromatic region for **1a**.

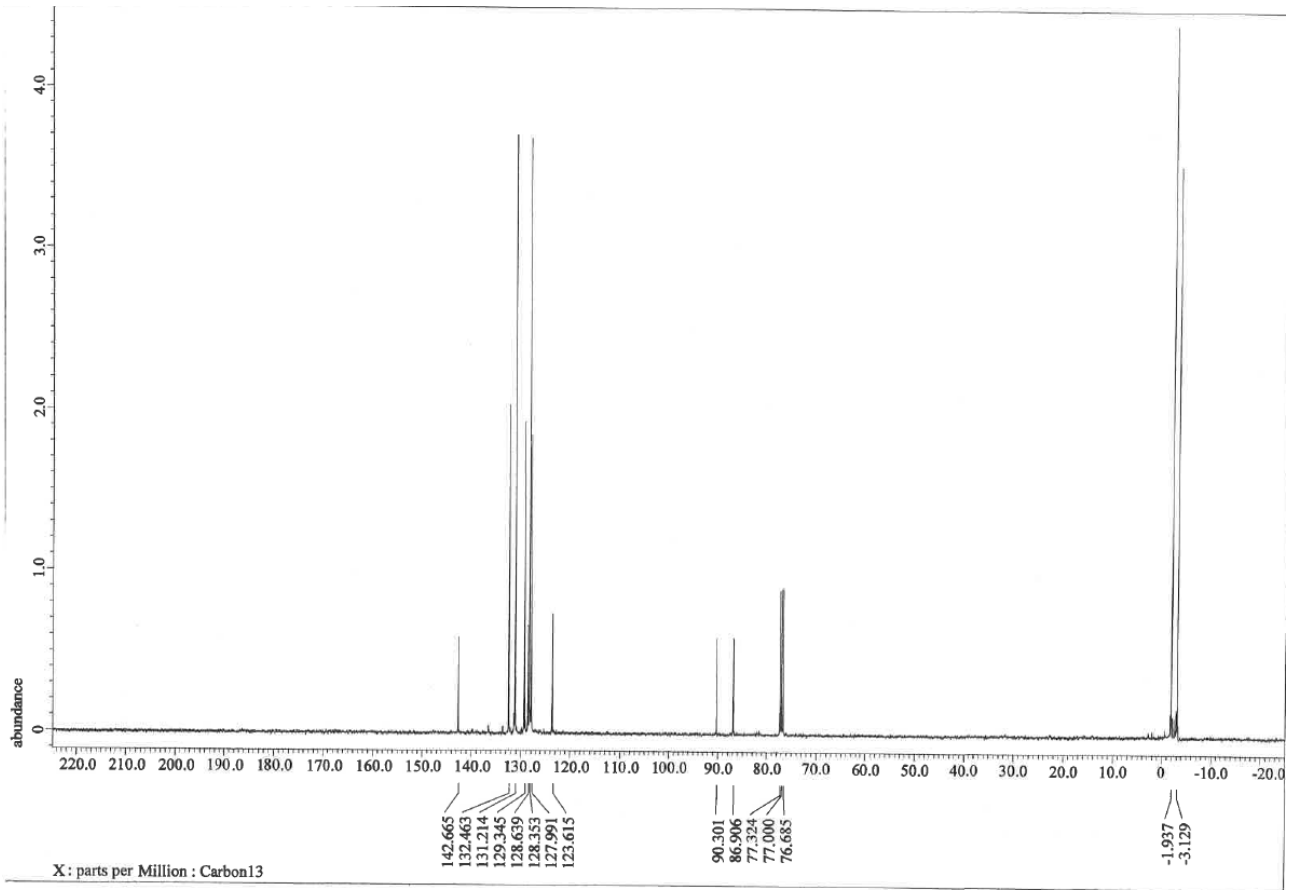

Figure S7. ^{13}C NMR spectrum of **1a** in $CDCl_3$.

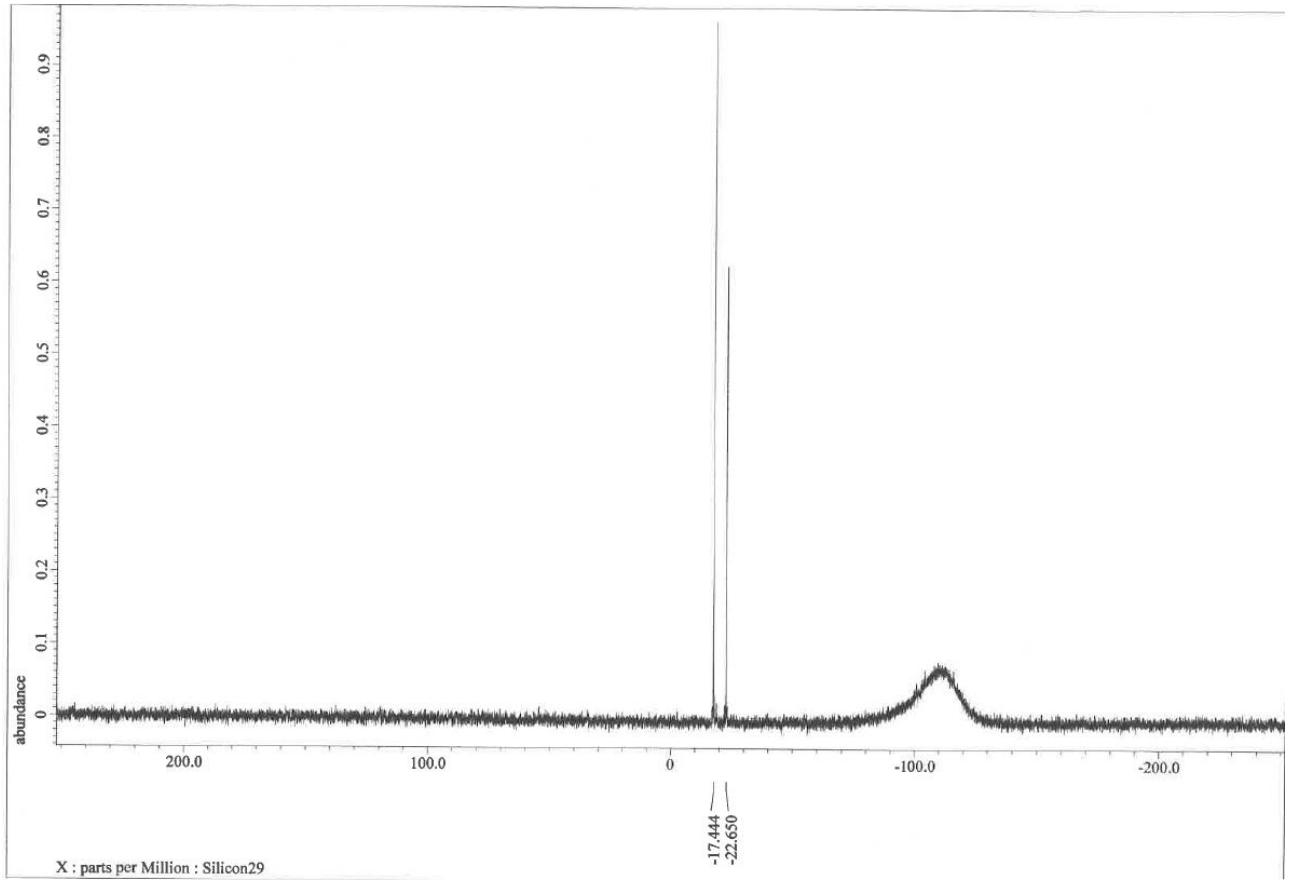

Figure S8. ^{29}Si NMR spectrum of **1a** in $CDCl_3$.

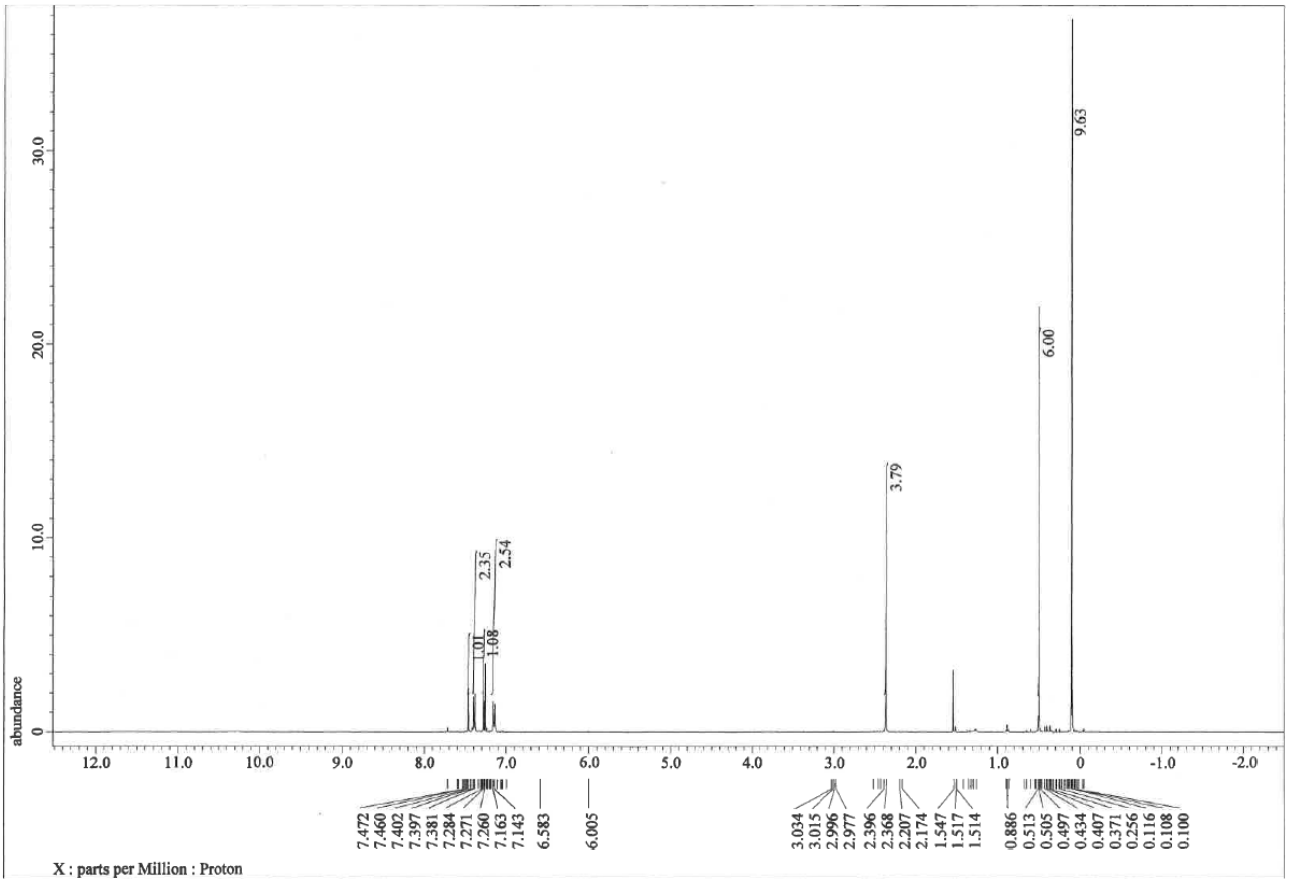

Figure S9. ^{1}H NMR spectrum of **1b** in $CDCl_3$.

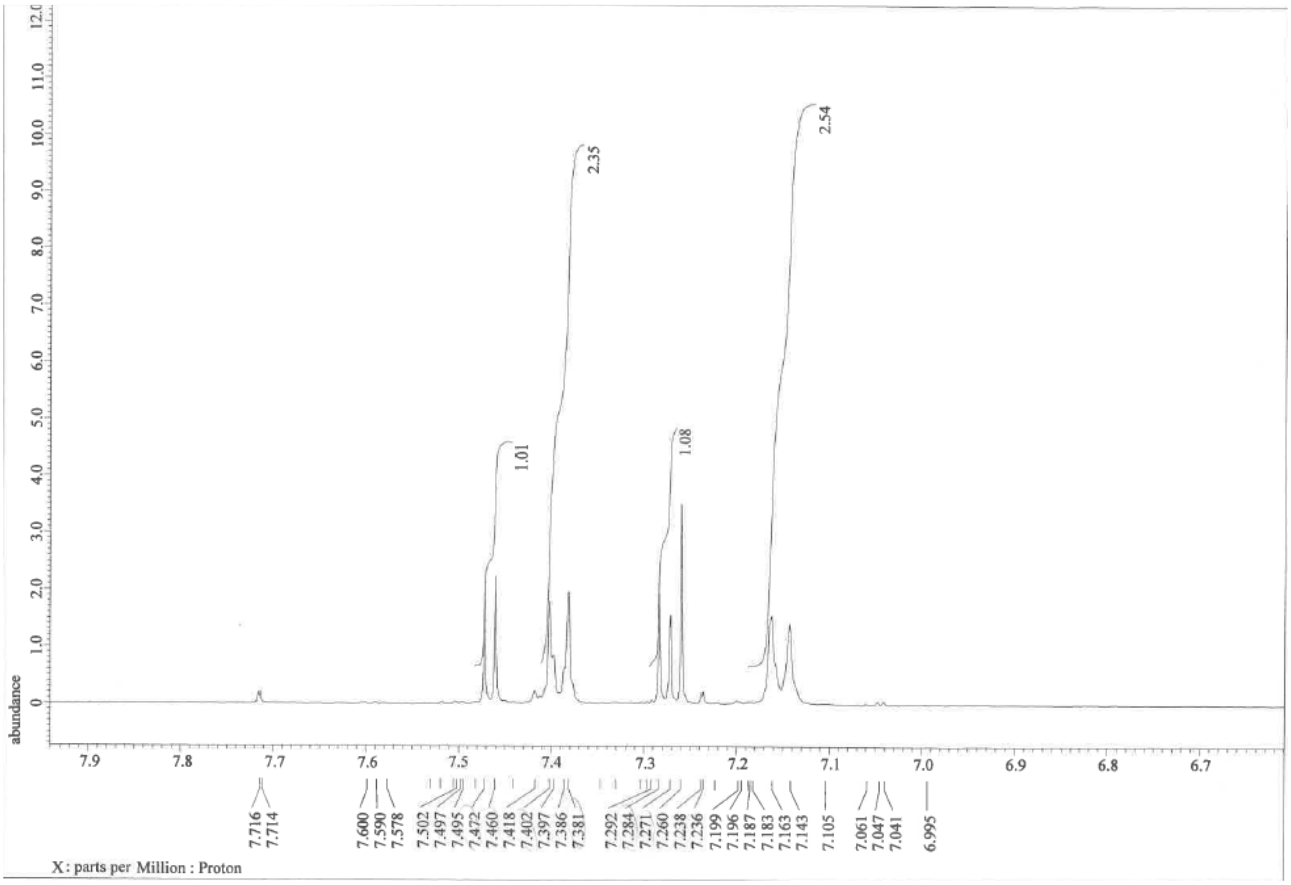

Figure S10. Enlarged view of the aromatic region for **1b**.

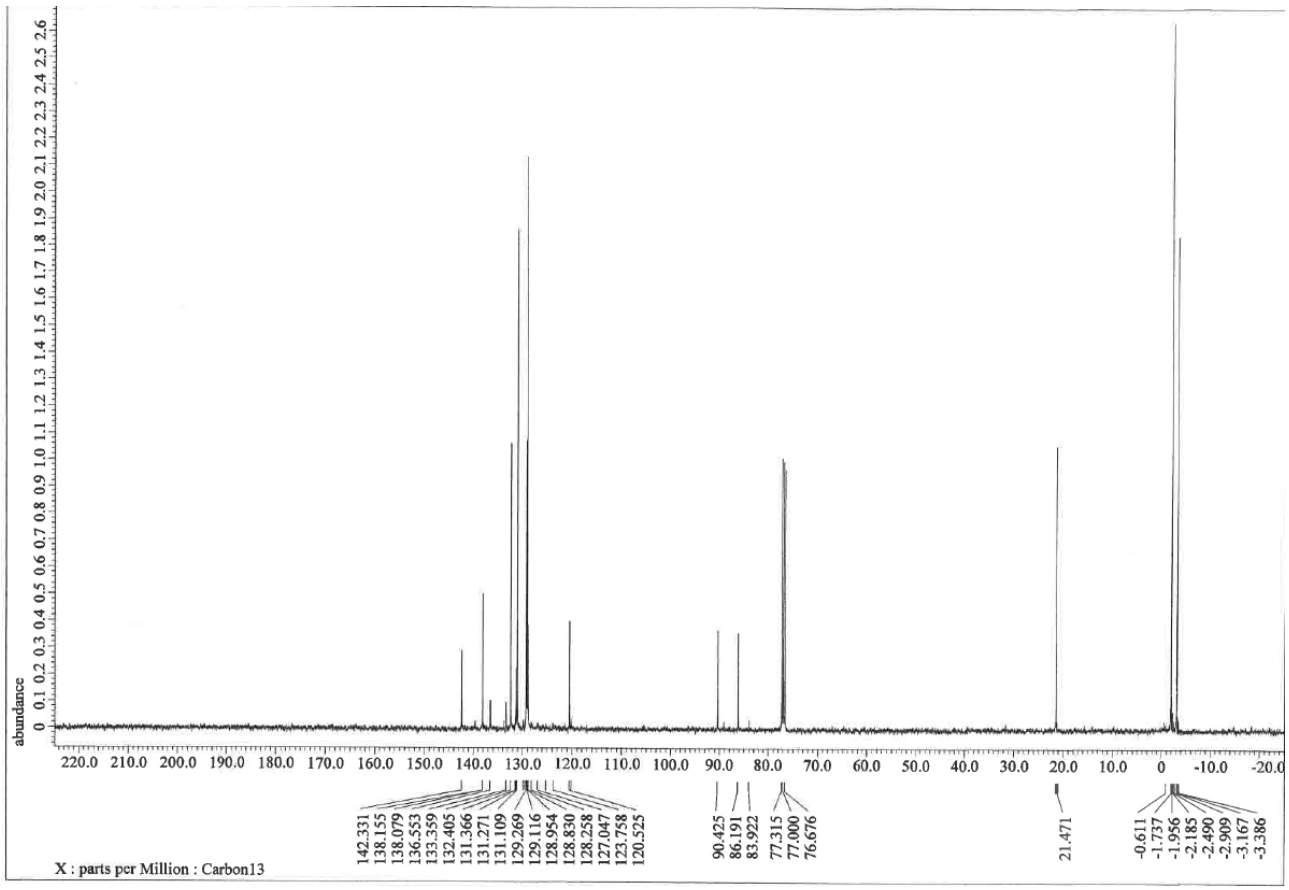

Figure S11. ^{13}C NMR spectrum of **1b** in $CDCl_3$.

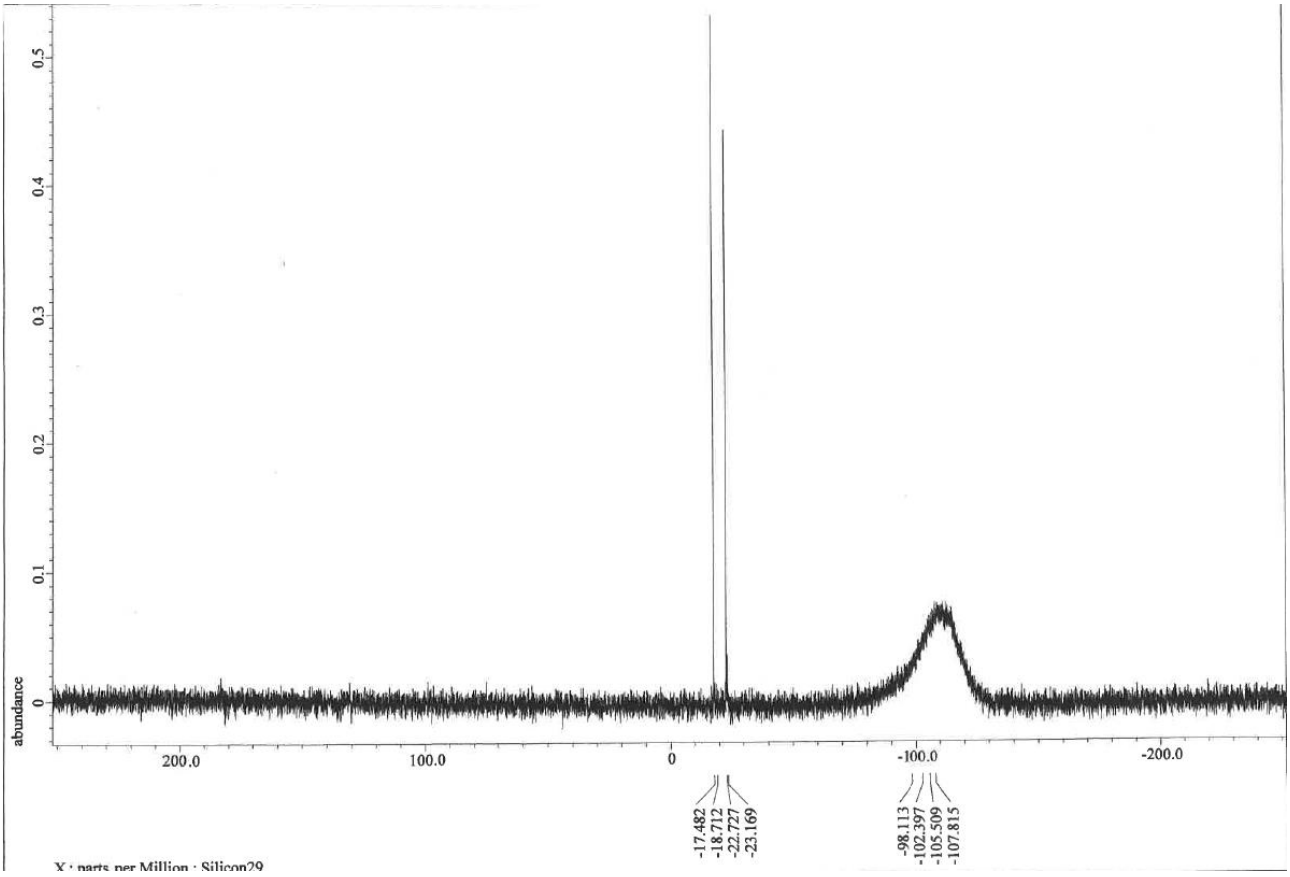

Figure S12. ^{29}Si NMR spectrum of **1b** in $CDCl_3$.

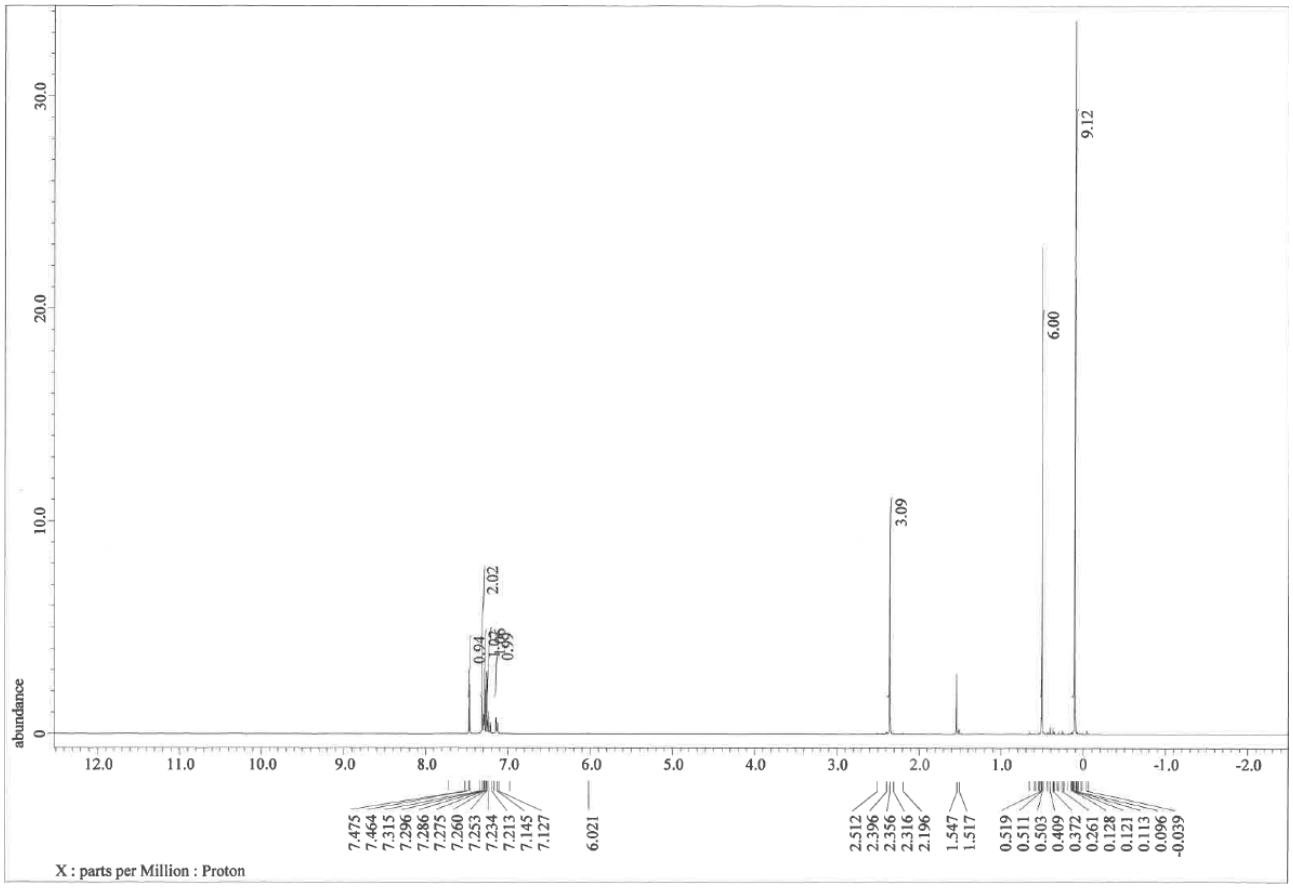

Figure S13. ^{1}H NMR spectrum of **1c** in $CDCl_3$.

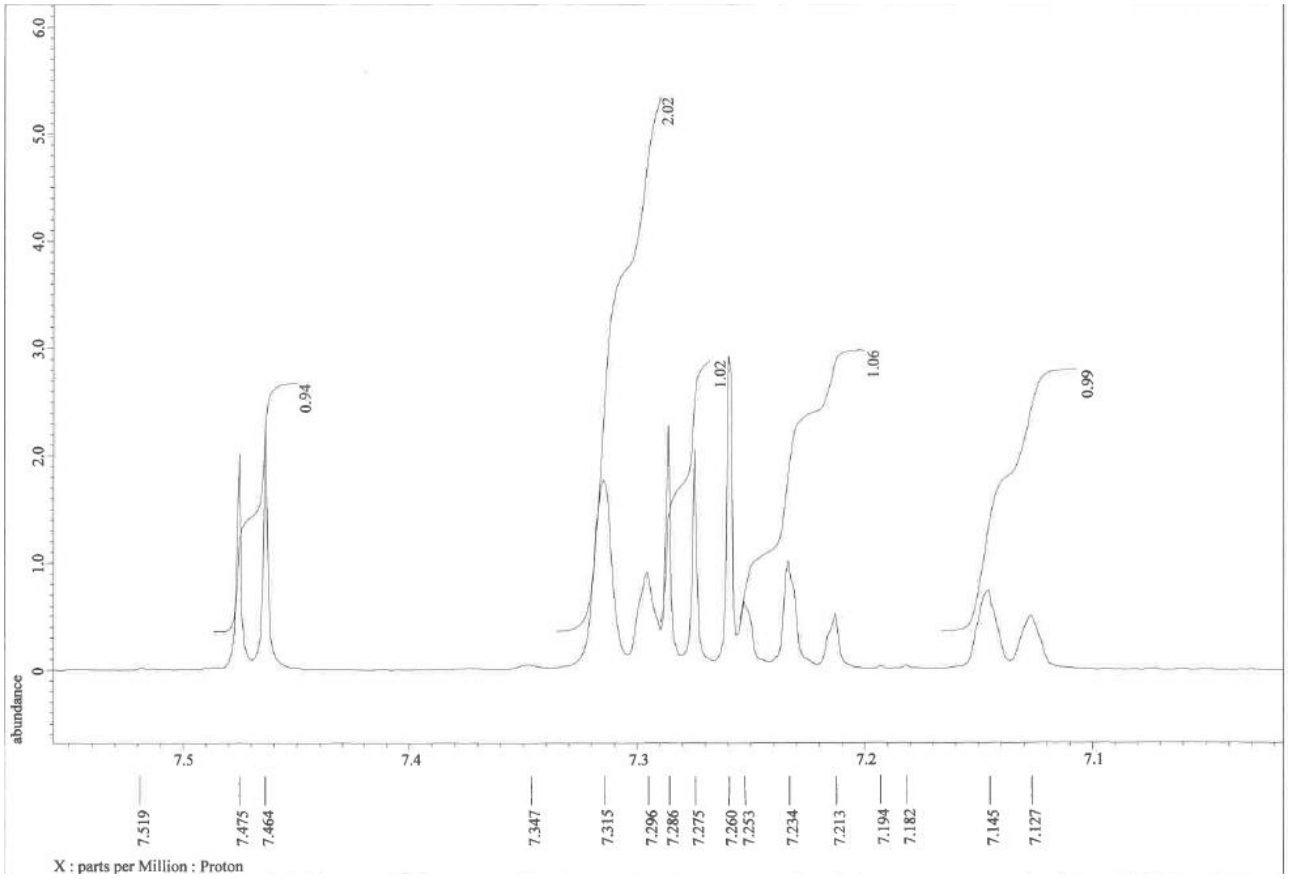

Figure S14. Enlarged view of the aromatic region for **1c**.

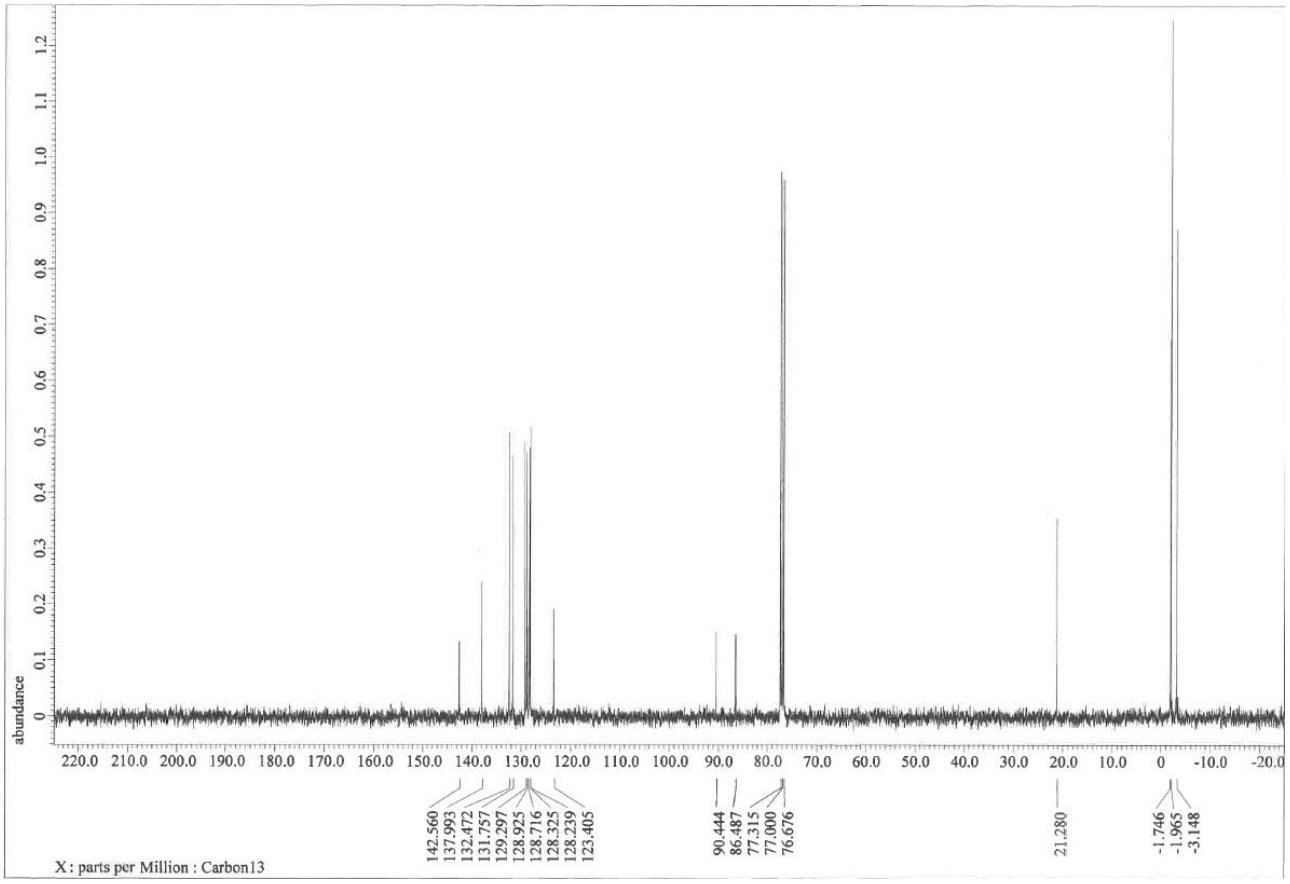

Figure S15. ^{13}C NMR spectrum of **1c** in $CDCl_3$.

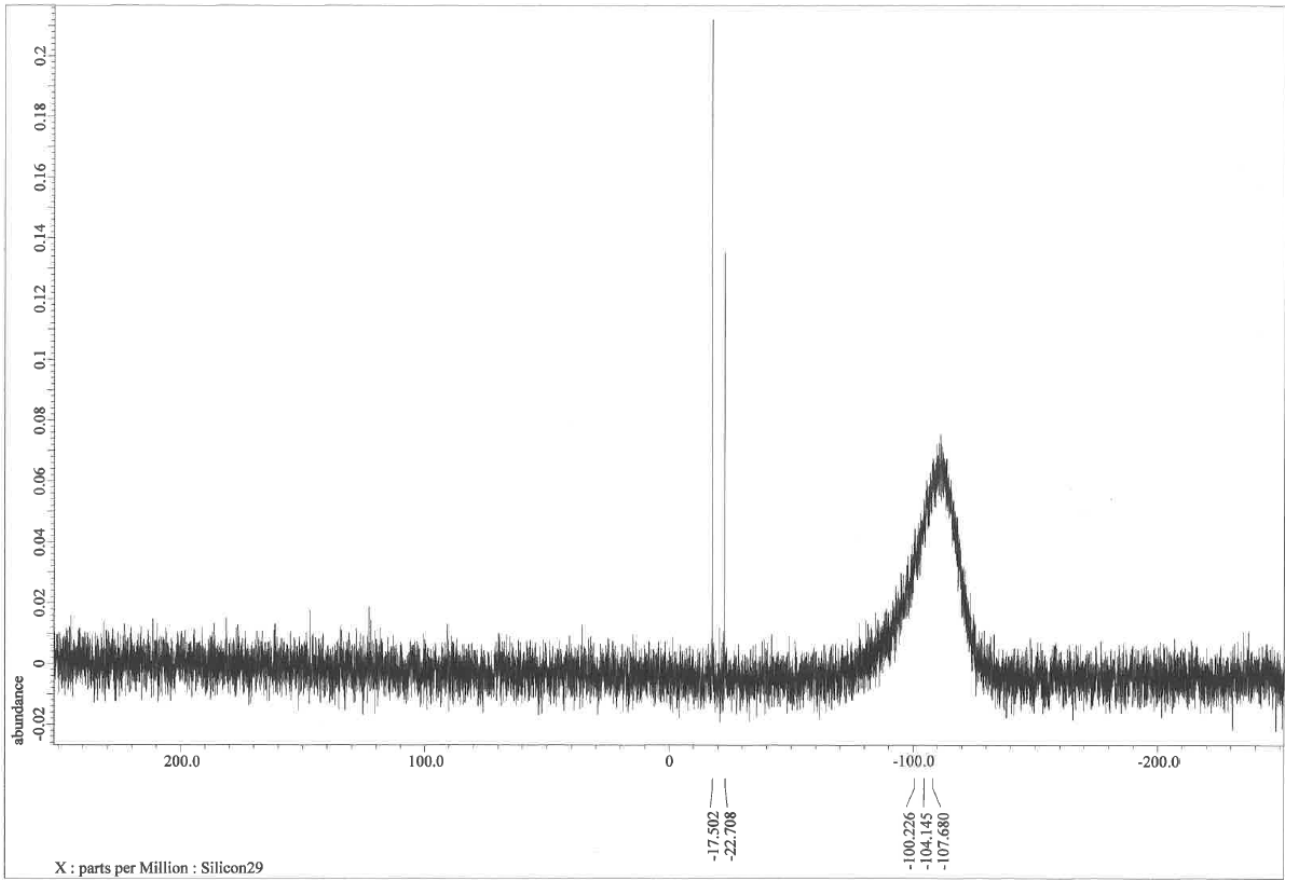

Figure S16. ^{29}Si NMR spectrum of **1c** in $CDCl_3$.

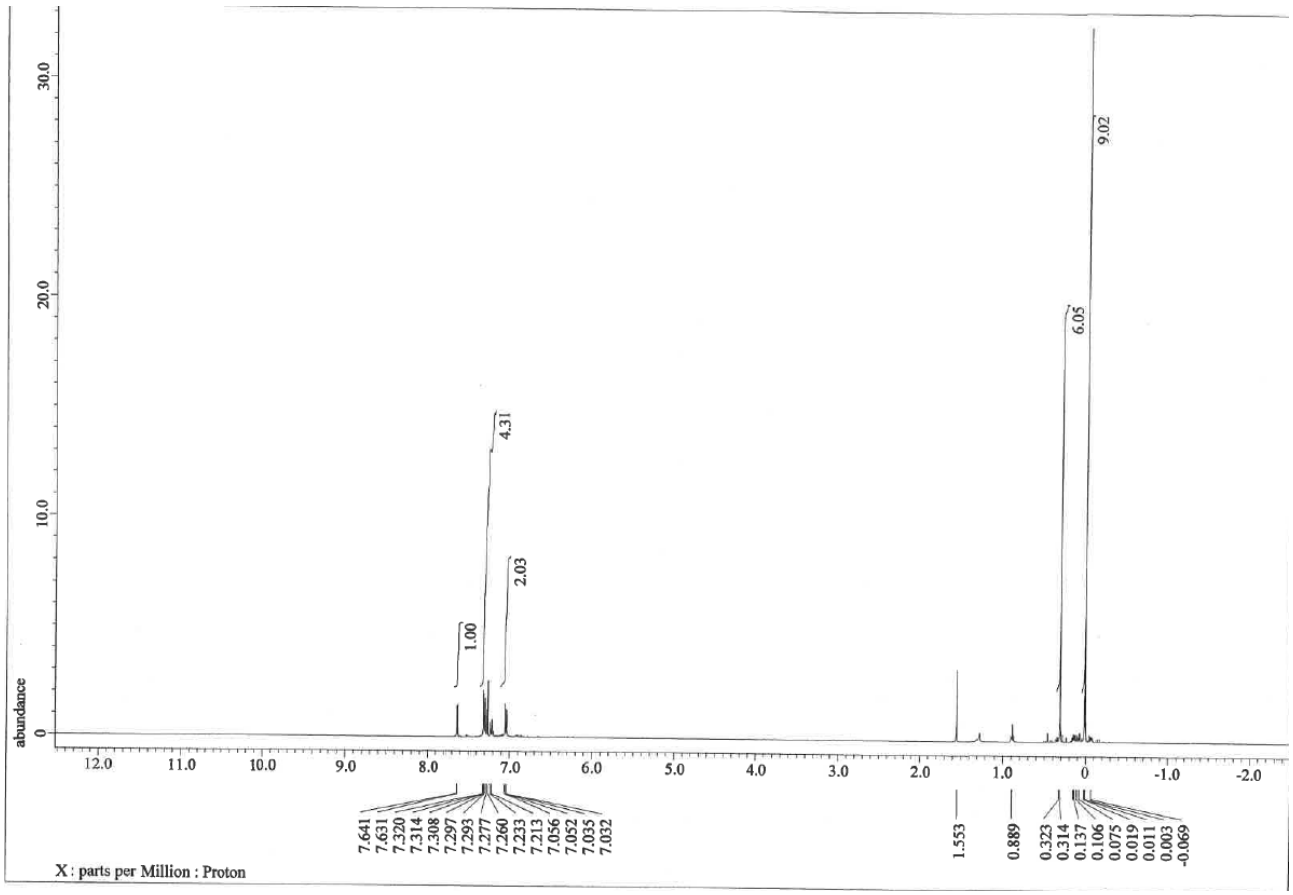

Figure S17. ^{1}H NMR spectrum of **2a** in $CDCl_3$.

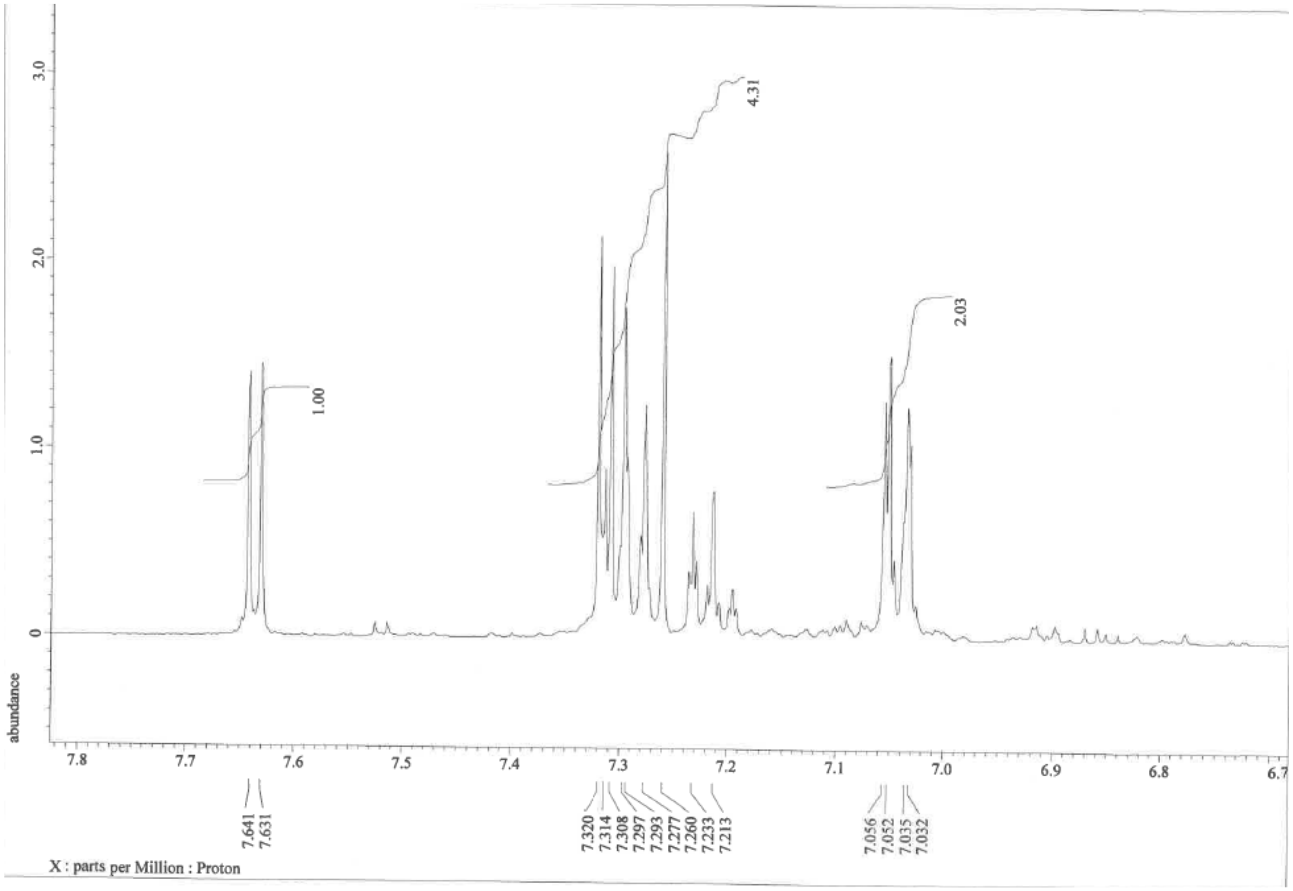

Figure S18. Enlarged view of the aromatic region for **2a**.

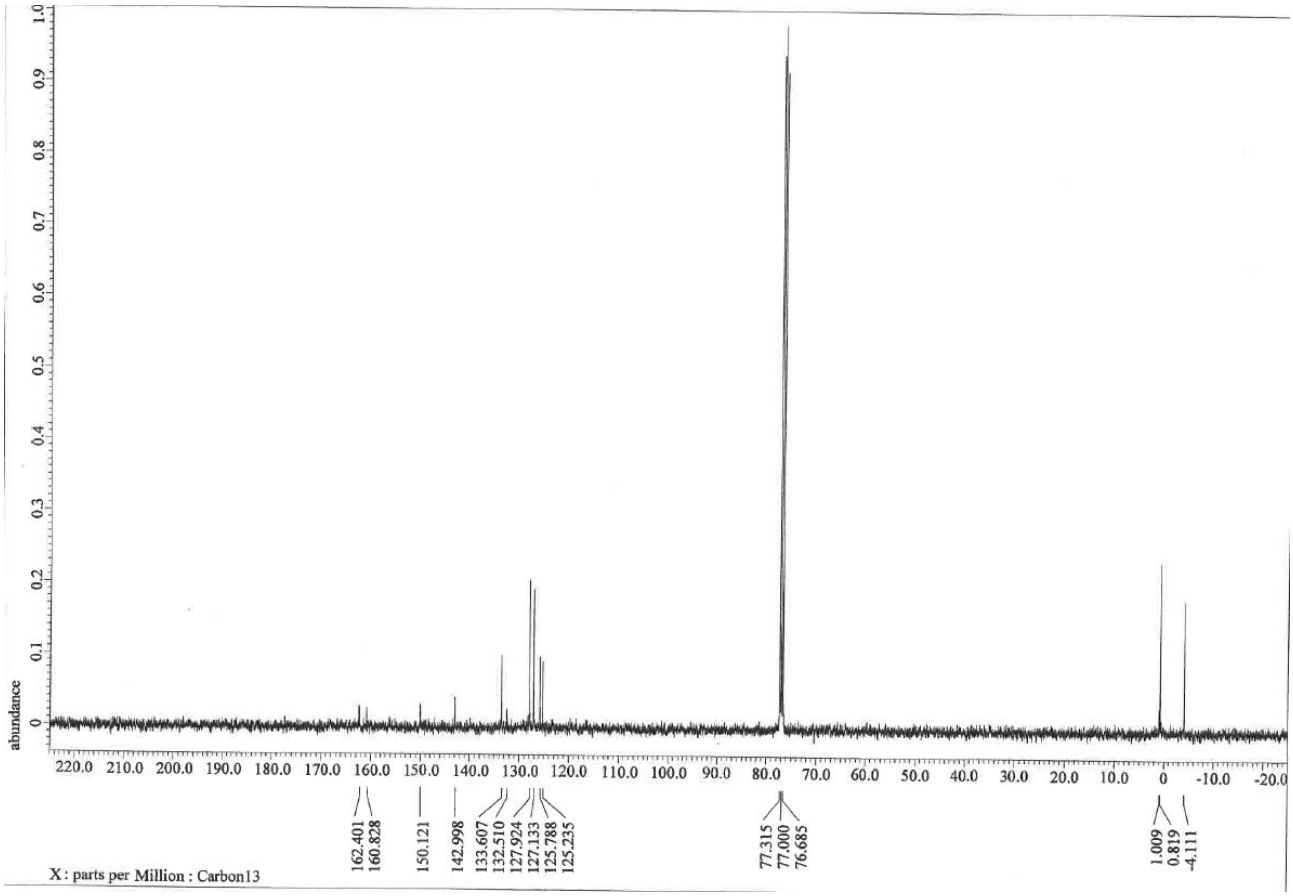

Figure S19. ^{13}C NMR spectrum of **2a** in $CDCl_3$.

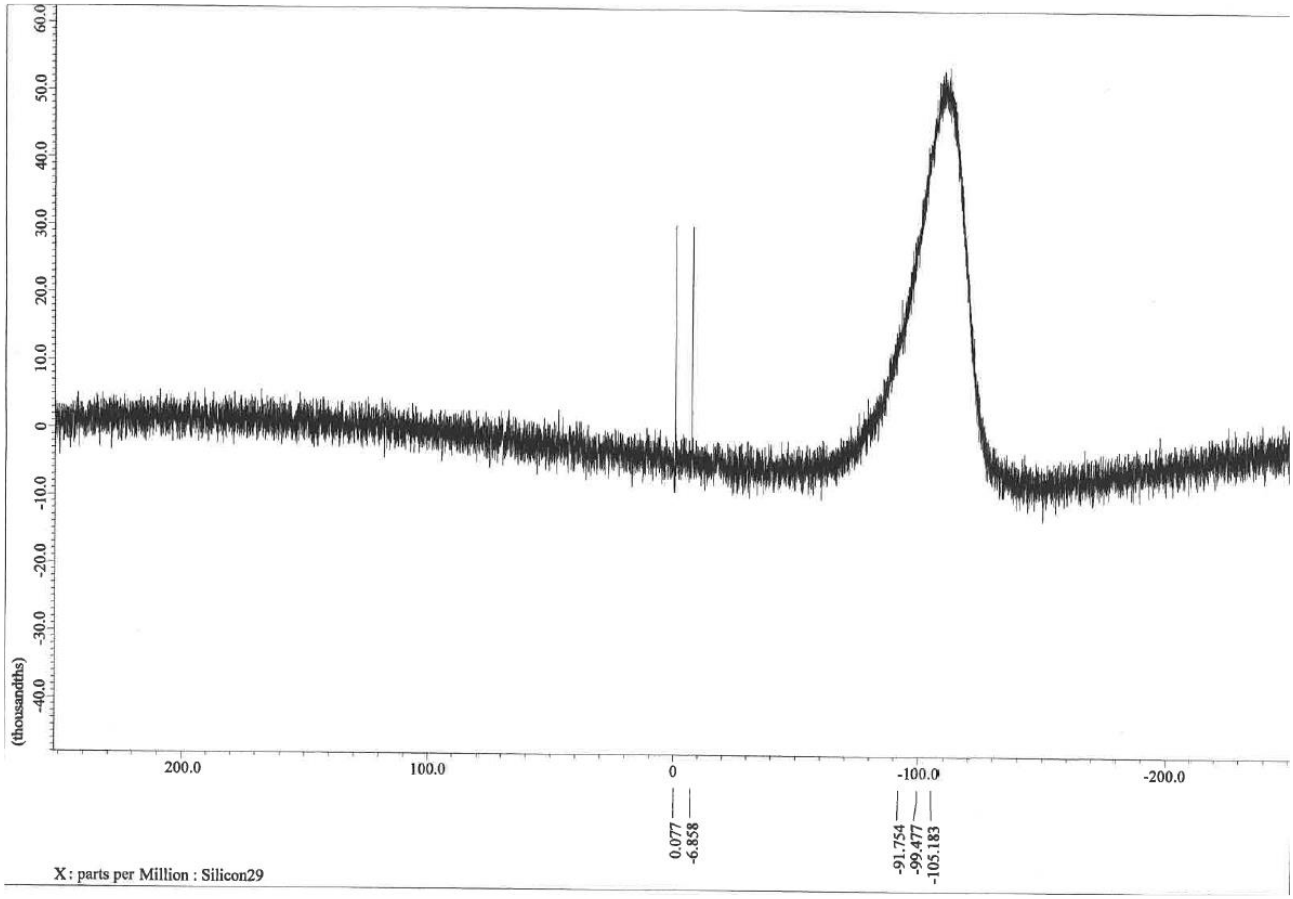

Figure S20. ^{29}Si NMR spectrum of **2a** in $CDCl_3$.

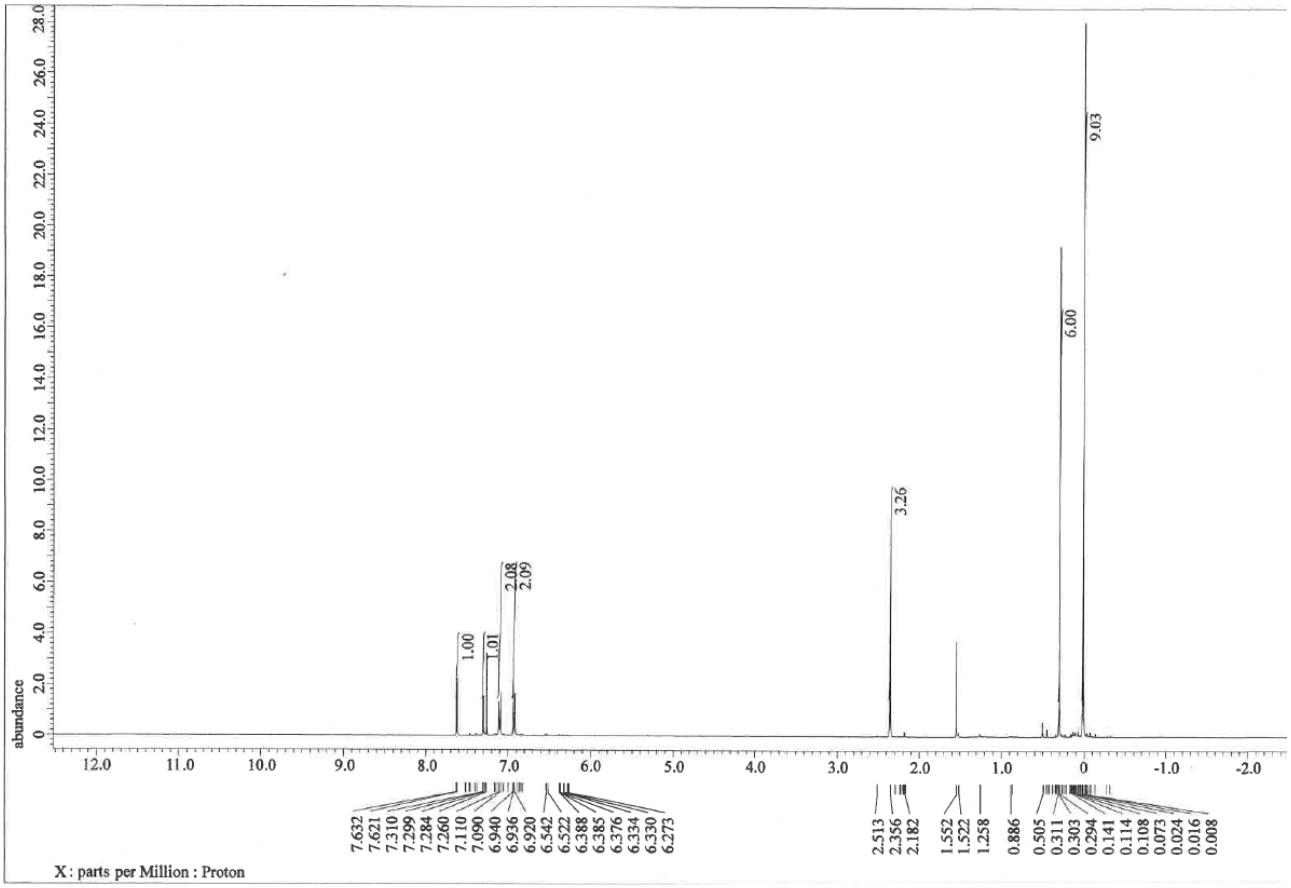

Figure S21. ^{1}H NMR spectrum of **2b** in $CDCl_3$.

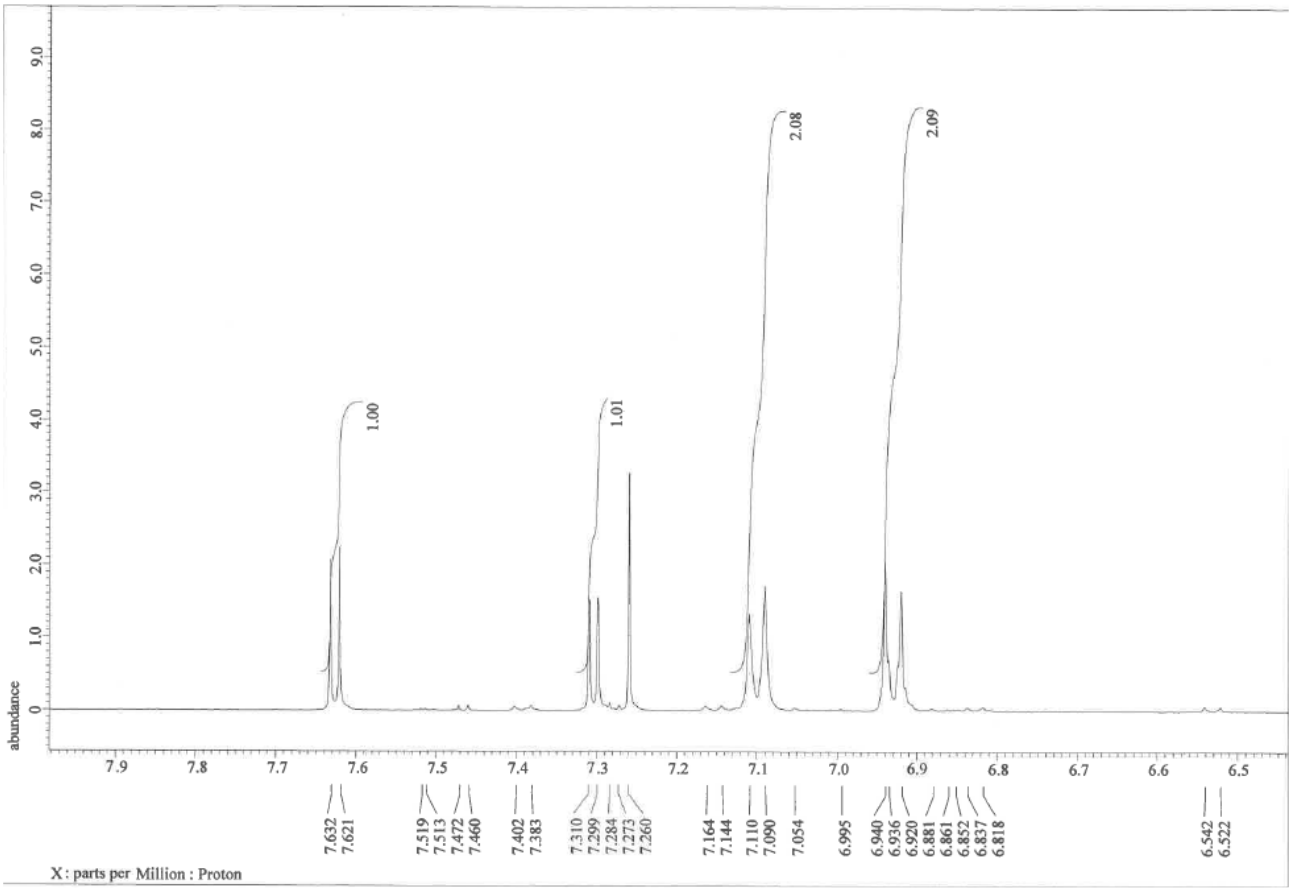

Figure S22. Enlarged view of the aromatic region for **2b**.

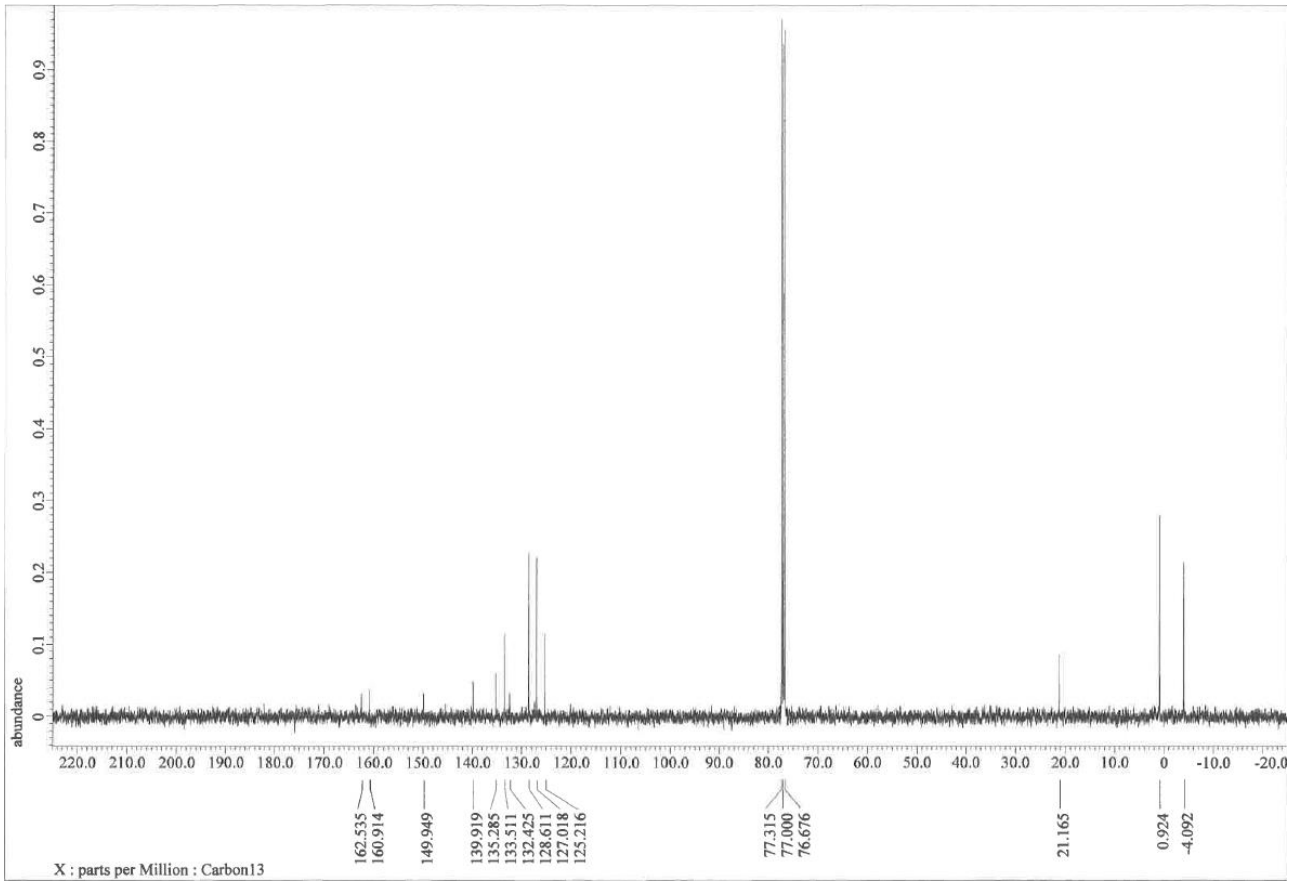

Figure S23. ^{13}C NMR spectrum of **2b** in $CDCl_3$.

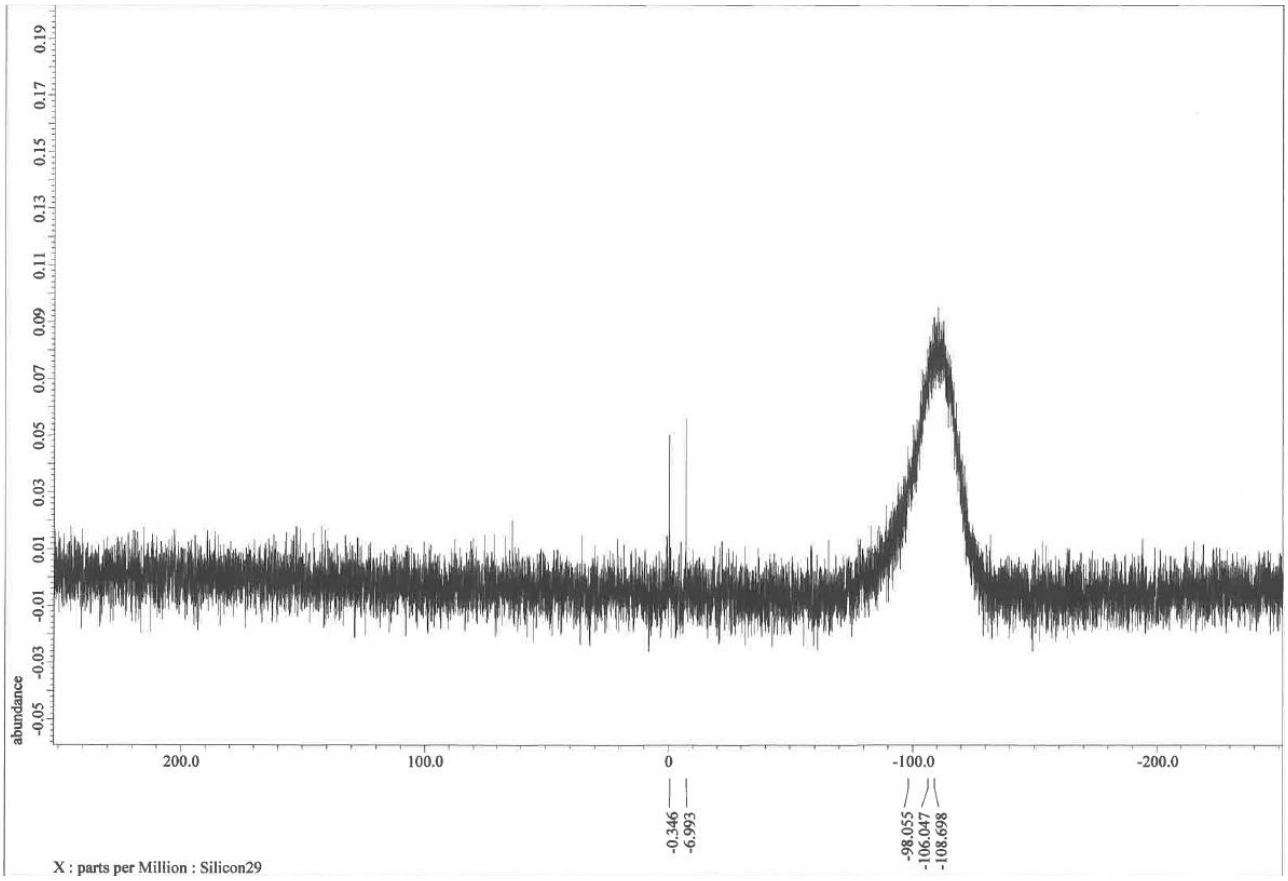

Figure S24. ^{29}Si NMR spectrum of **2b** in $CDCl_3$.

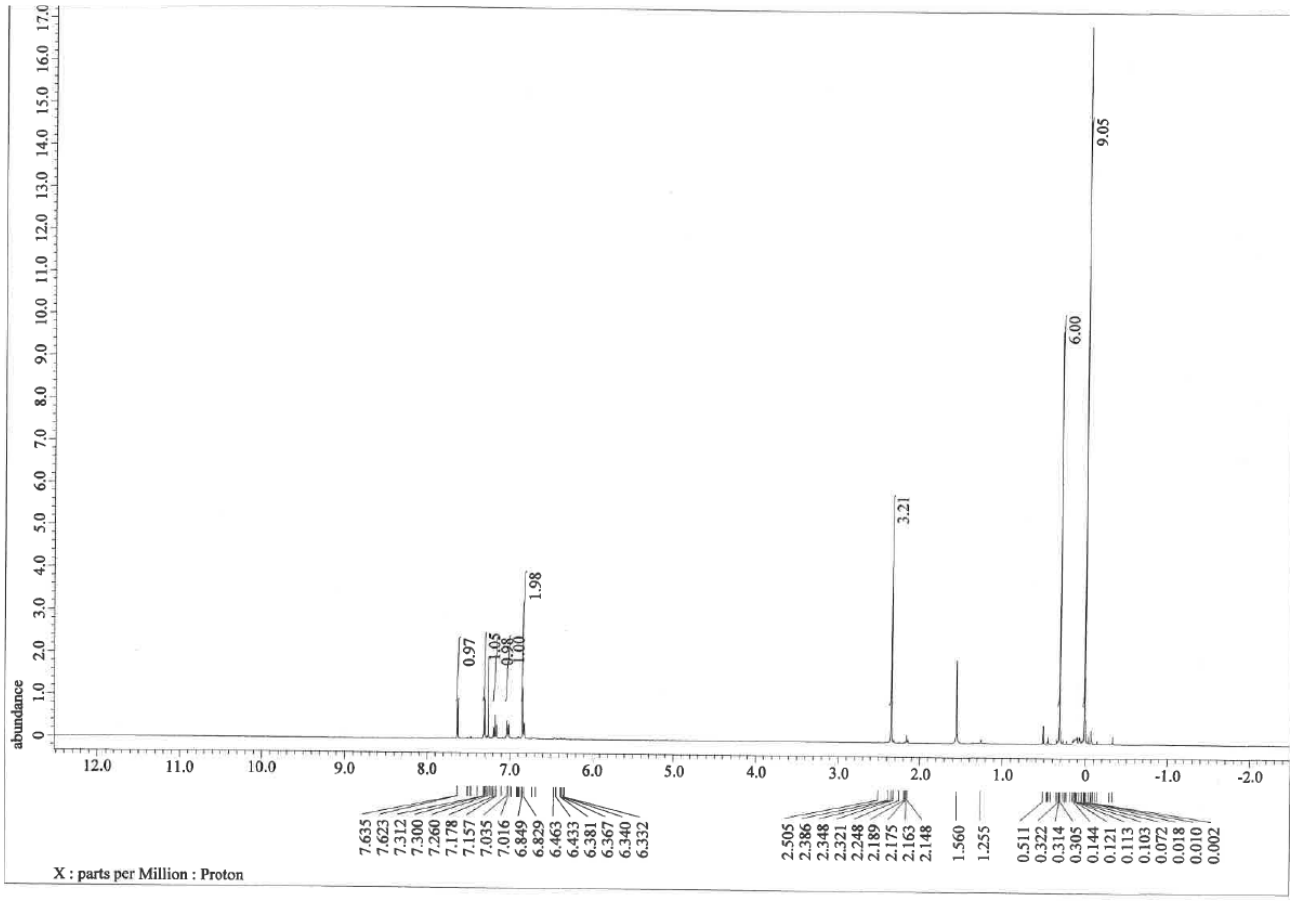

Figure S25. ^{1}H NMR spectrum of **2c** in $CDCl_3$.

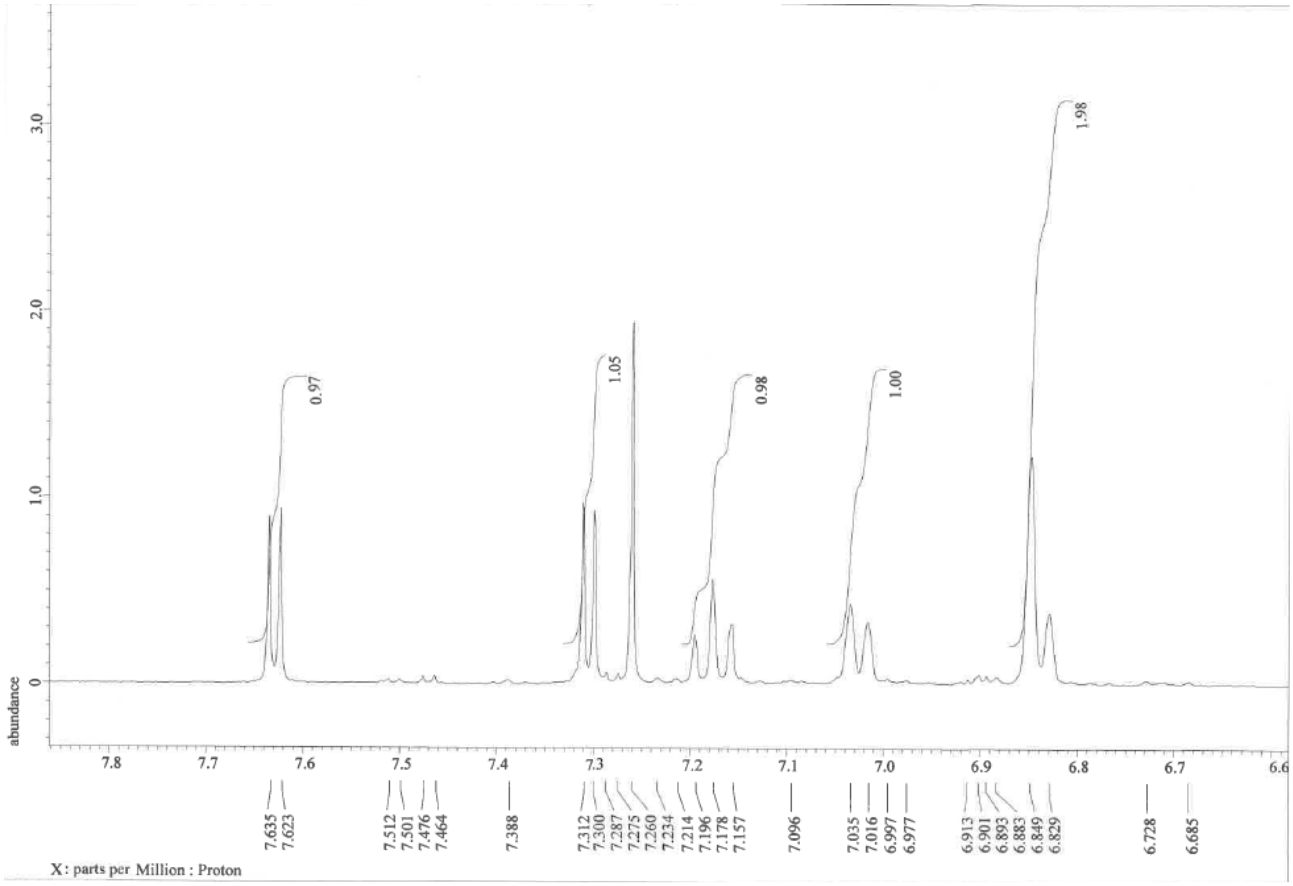

Figure S26. Enlarged view of the aromatic region for **2c**.

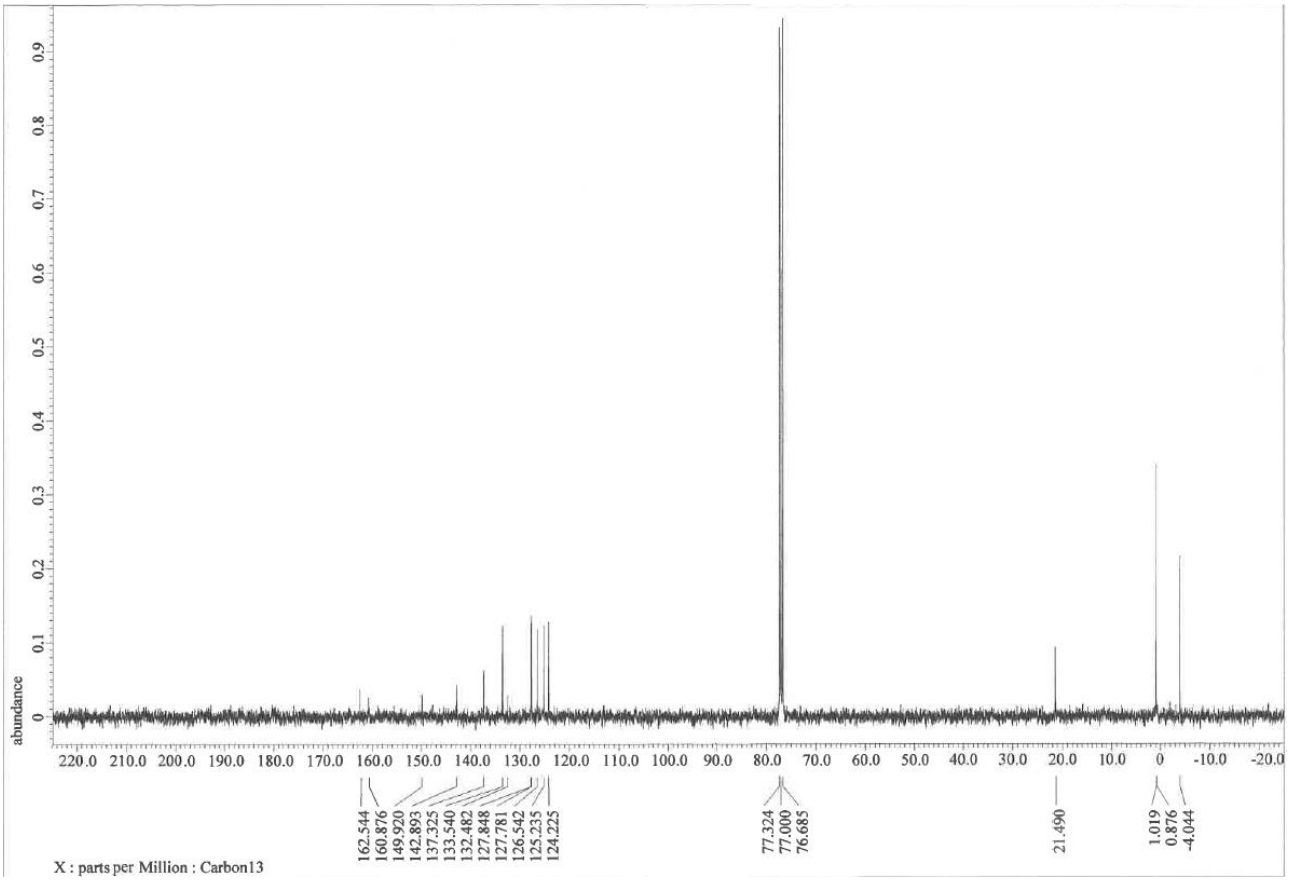

Figure S27. ^{13}C NMR spectrum of **2c** in $CDCl_3$.

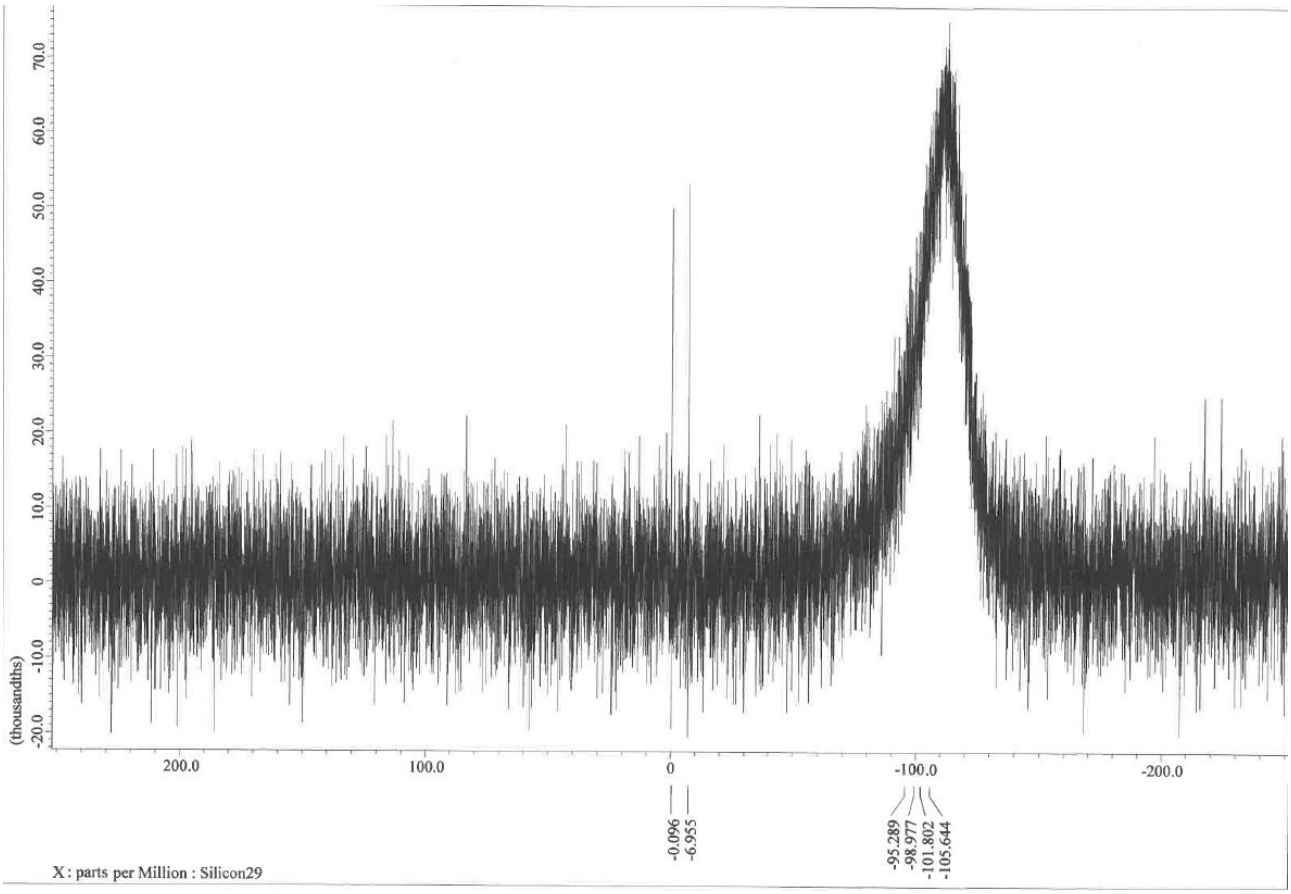

Figure S28. ^{29}Si NMR spectrum of **2c** in $CDCl_3$.

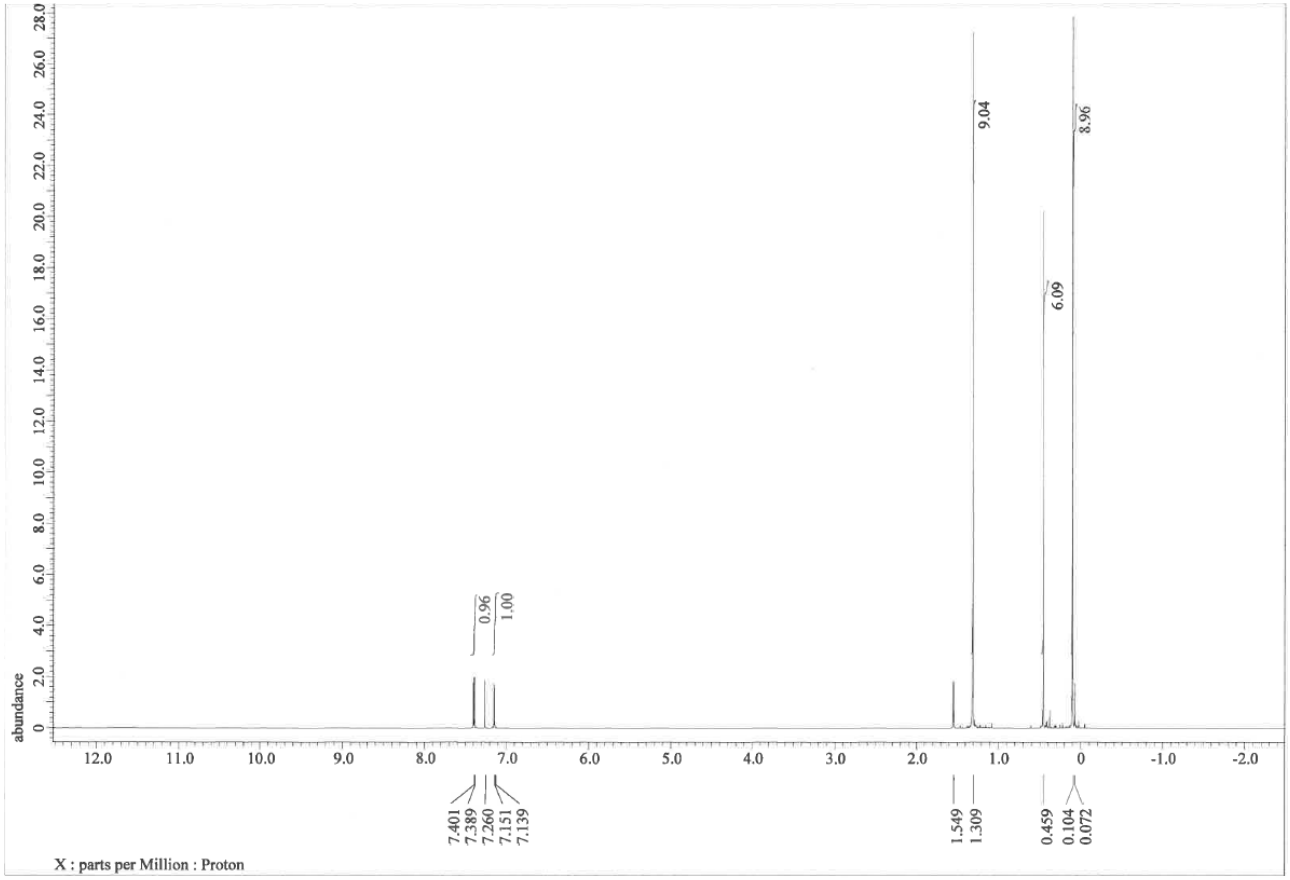

Figure S29. ^{1}H NMR spectrum of **3** in $CDCl_3$.

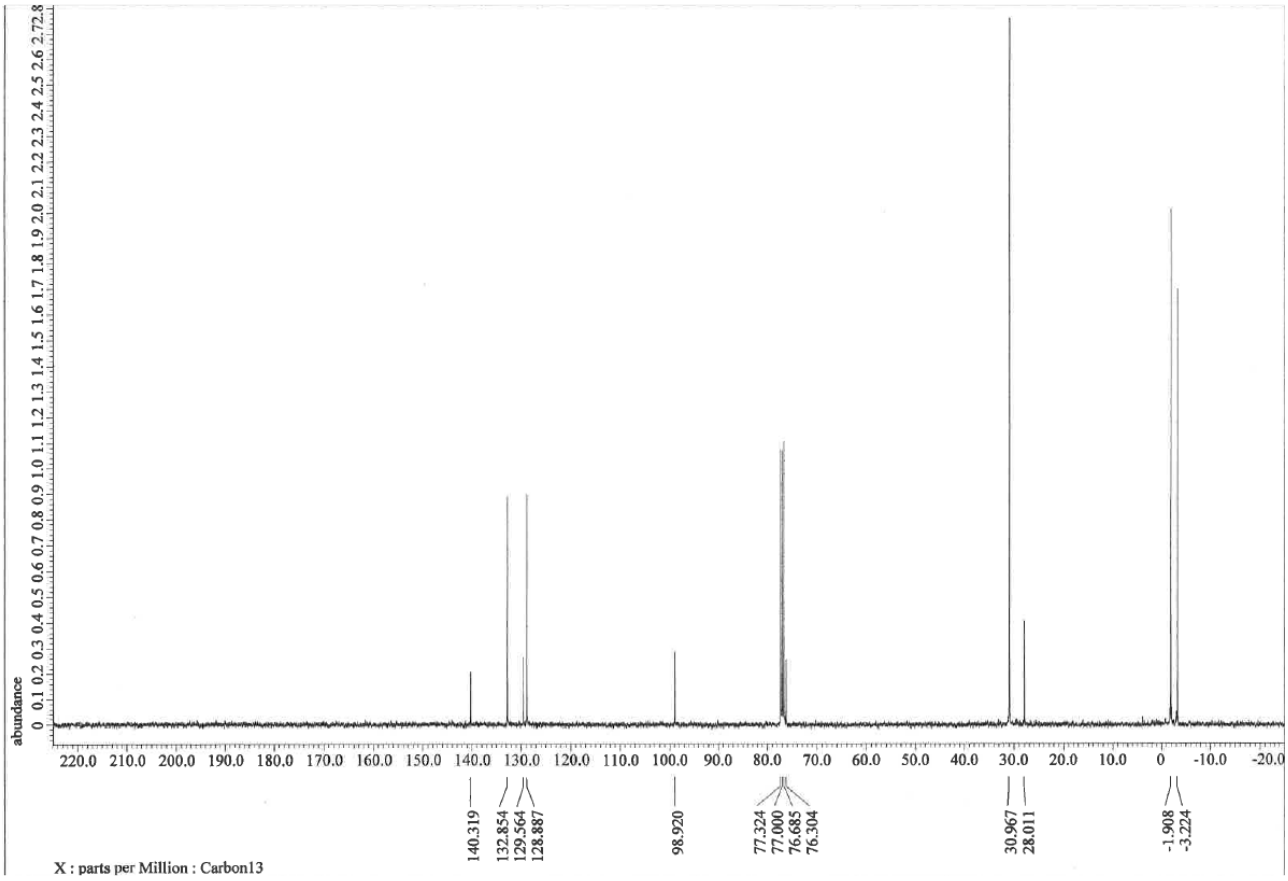

Figure S30. ^{13}C NMR spectrum of **3** in $CDCl_3$.

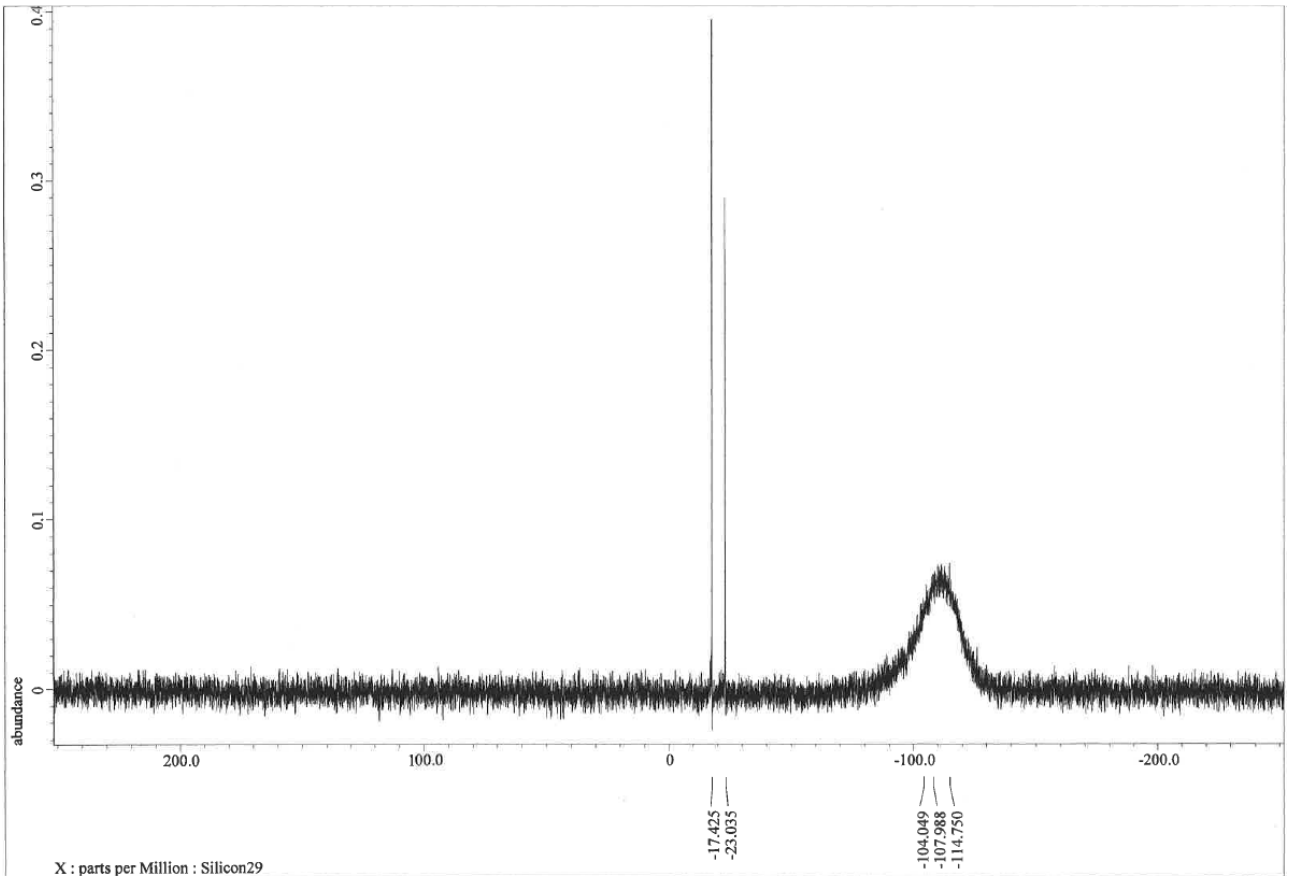

Figure S31. ^{29}Si NMR spectrum of **3** in $CDCl_3$.

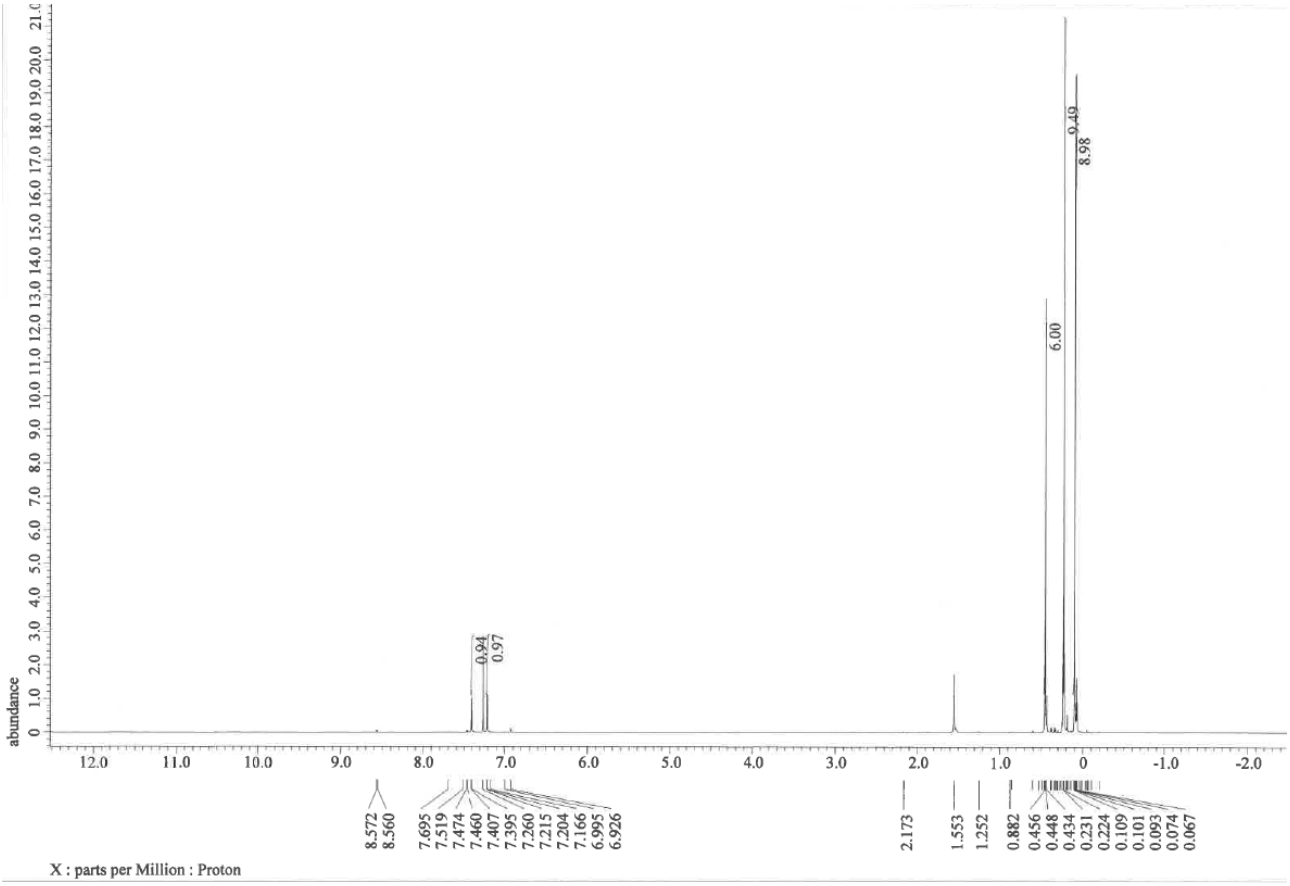

Figure S32. ^{1}H NMR spectrum of **4** in $CDCl_3$.

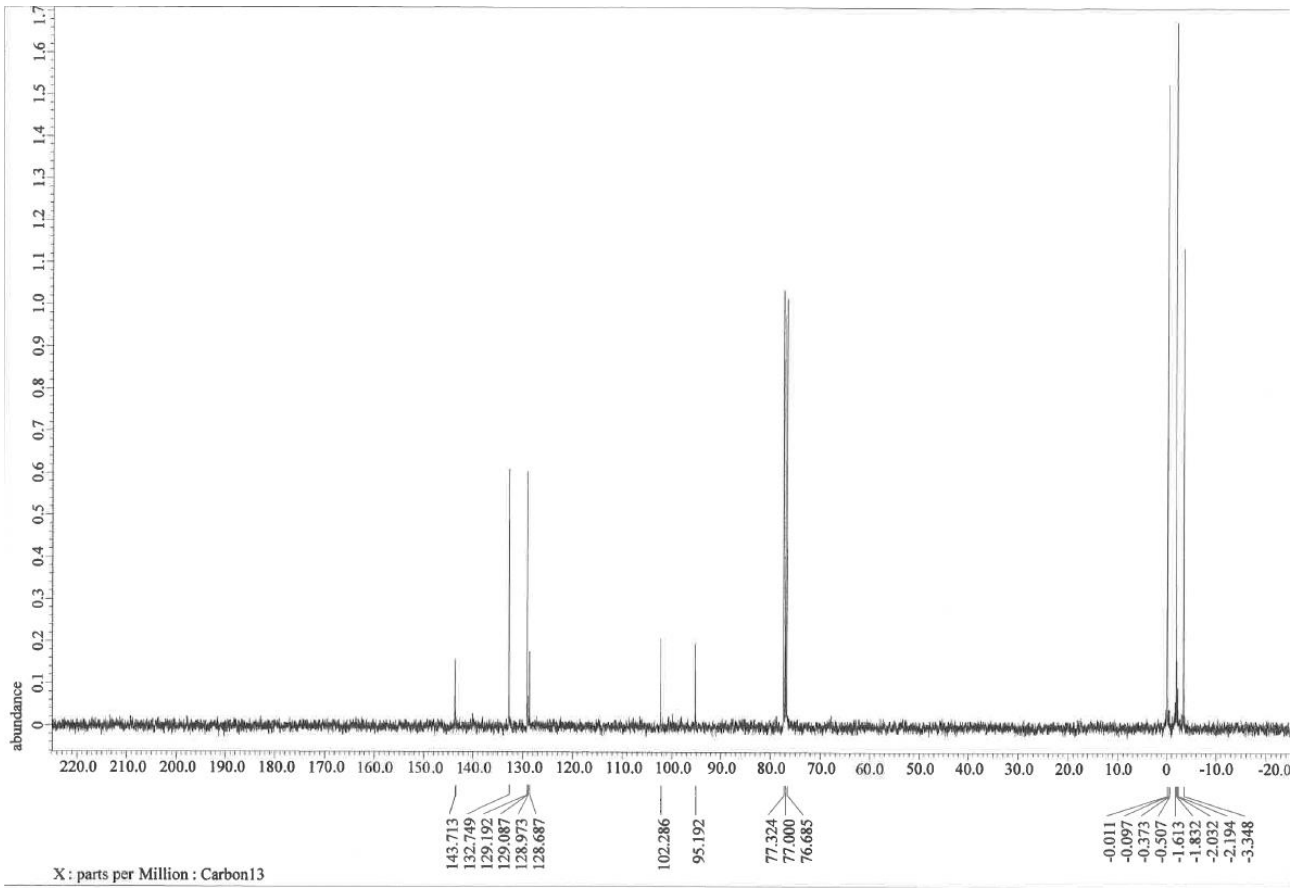

Figure S33. ^{13}C NMR spectrum of **4** in $CDCl_3$.

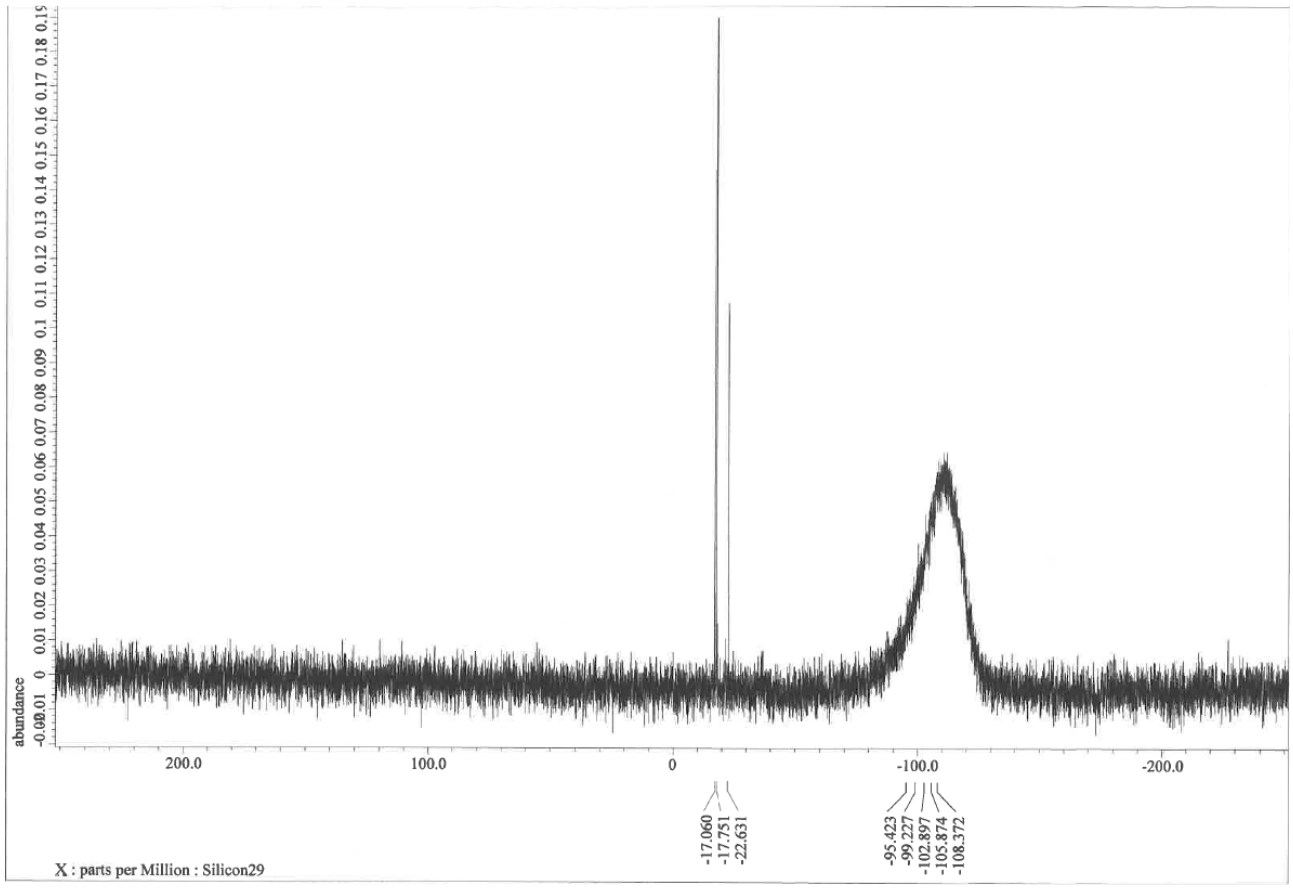

Figure S34. ^{29}Si NMR spectrum of **4** in $CDCl_3$.

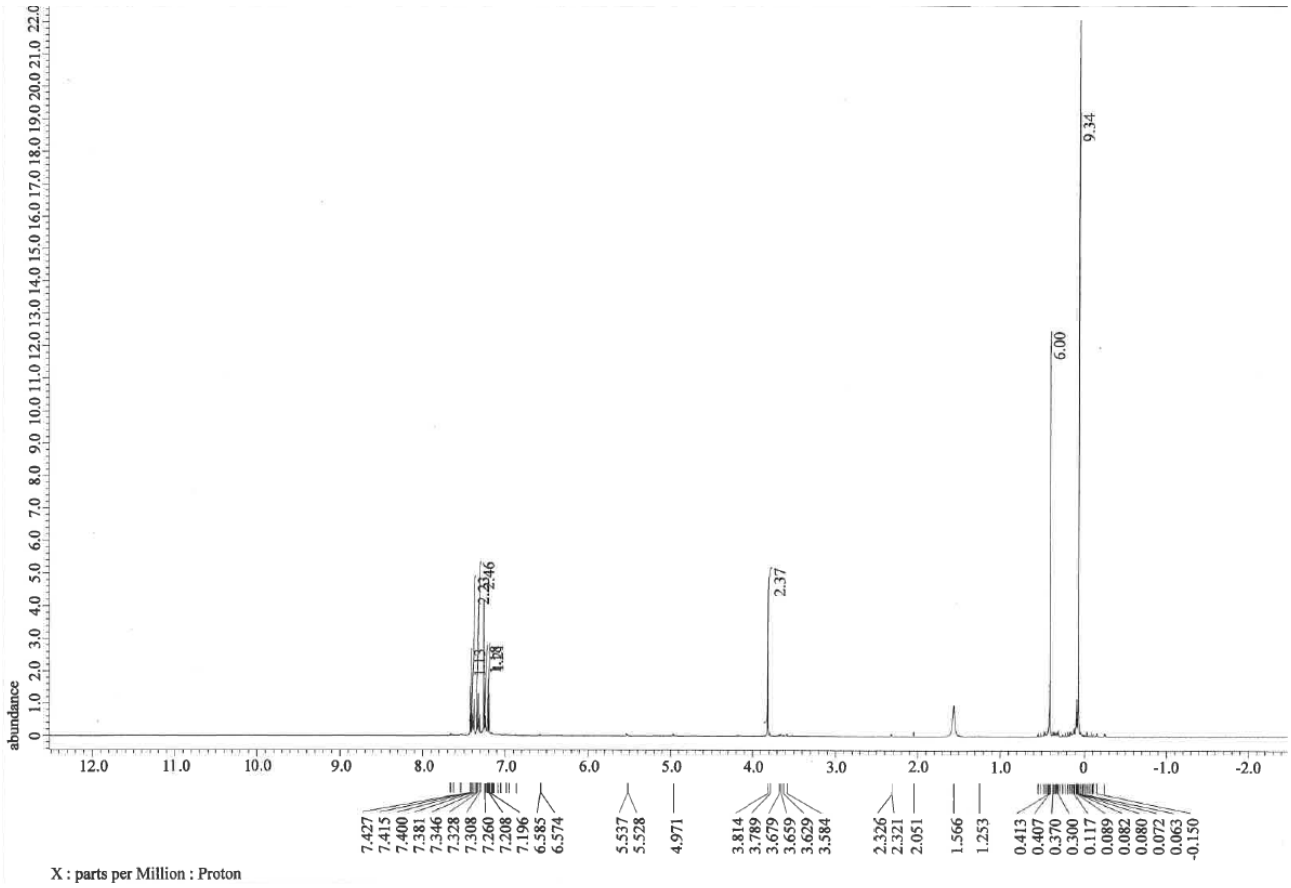

Figure S35. ^{1}H NMR spectrum of **5** in $CDCl_3$.

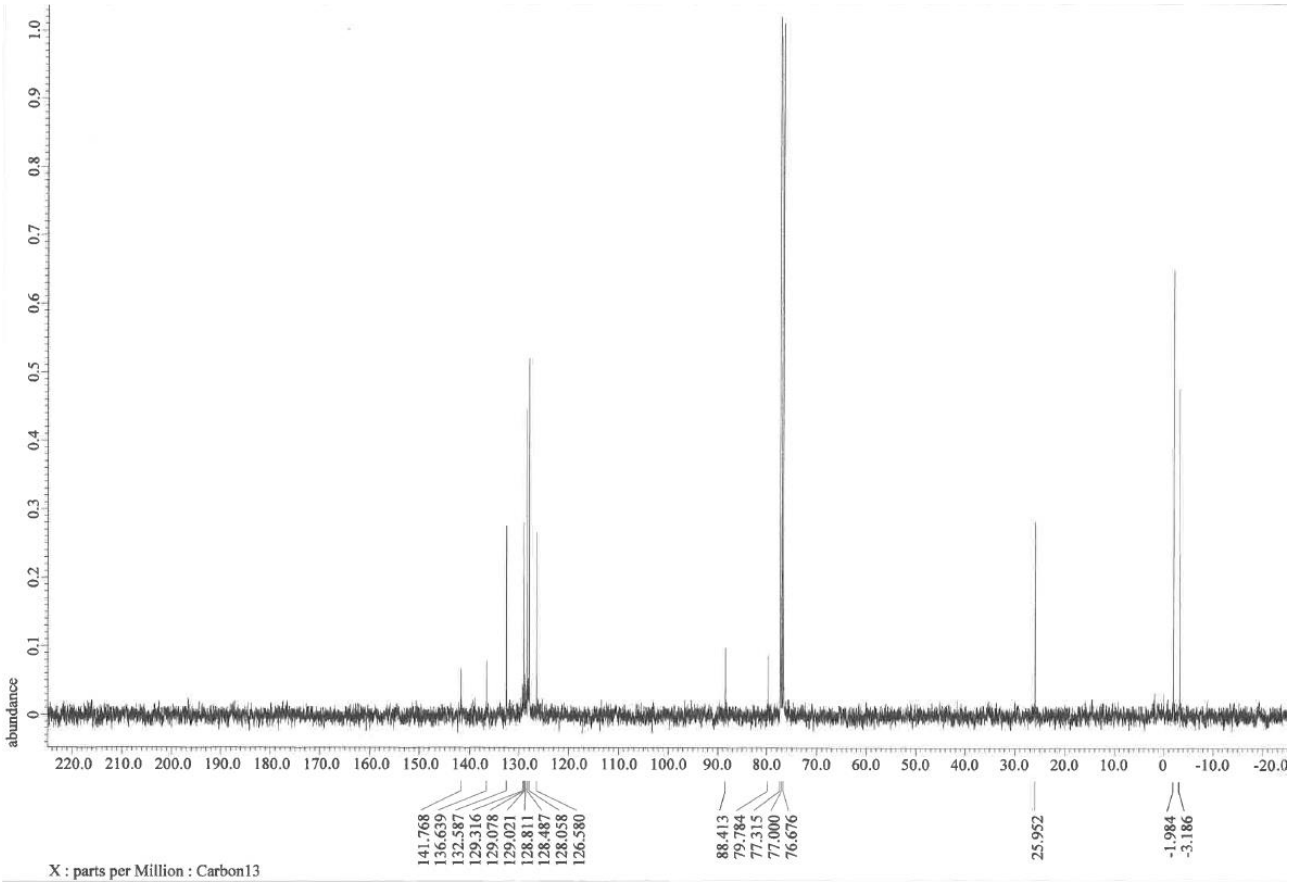

Figure S36. ^{13}C NMR spectrum of **5** in $CDCl_3$.

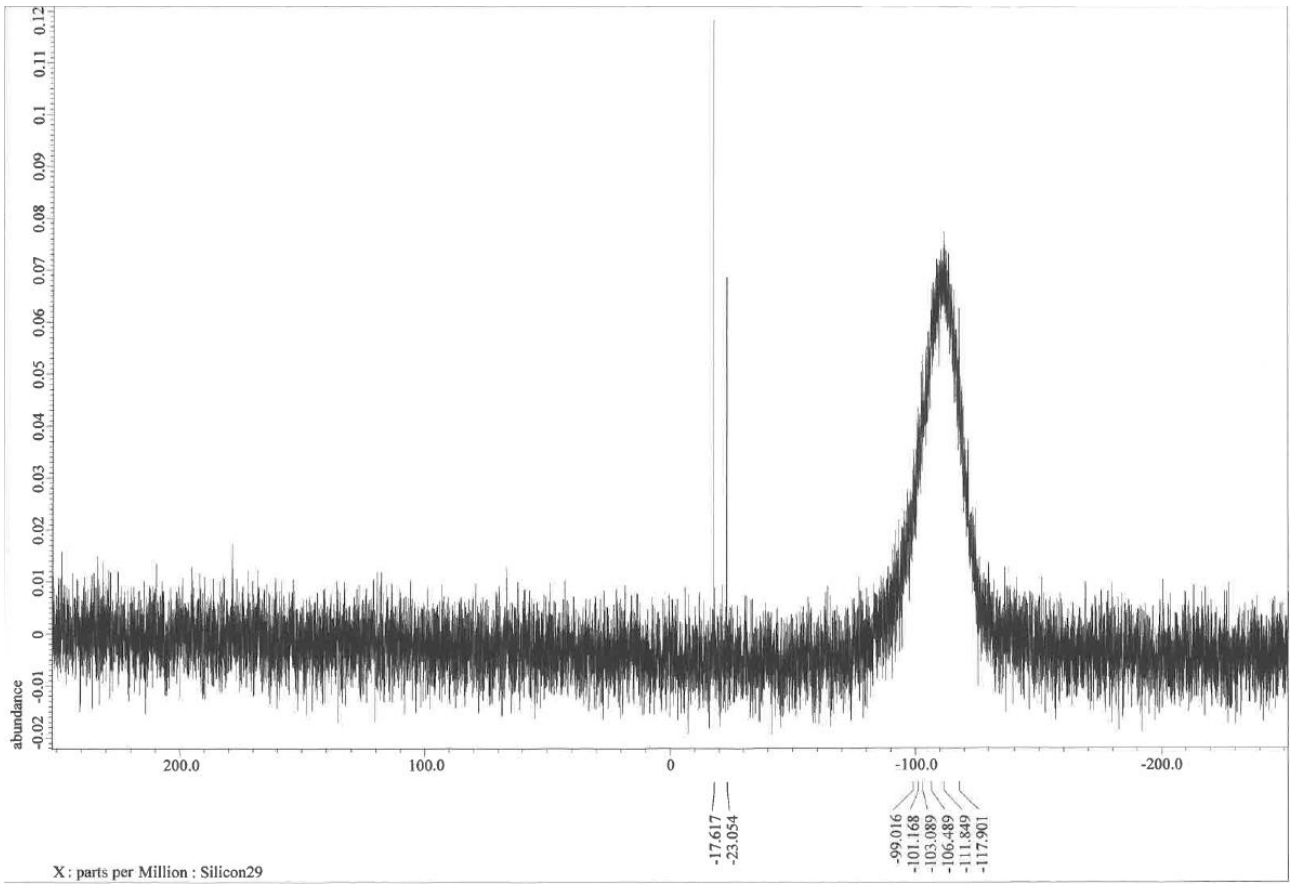

Figure S37. ^{29}Si NMR spectrum of **5** in $CDCl_3$.

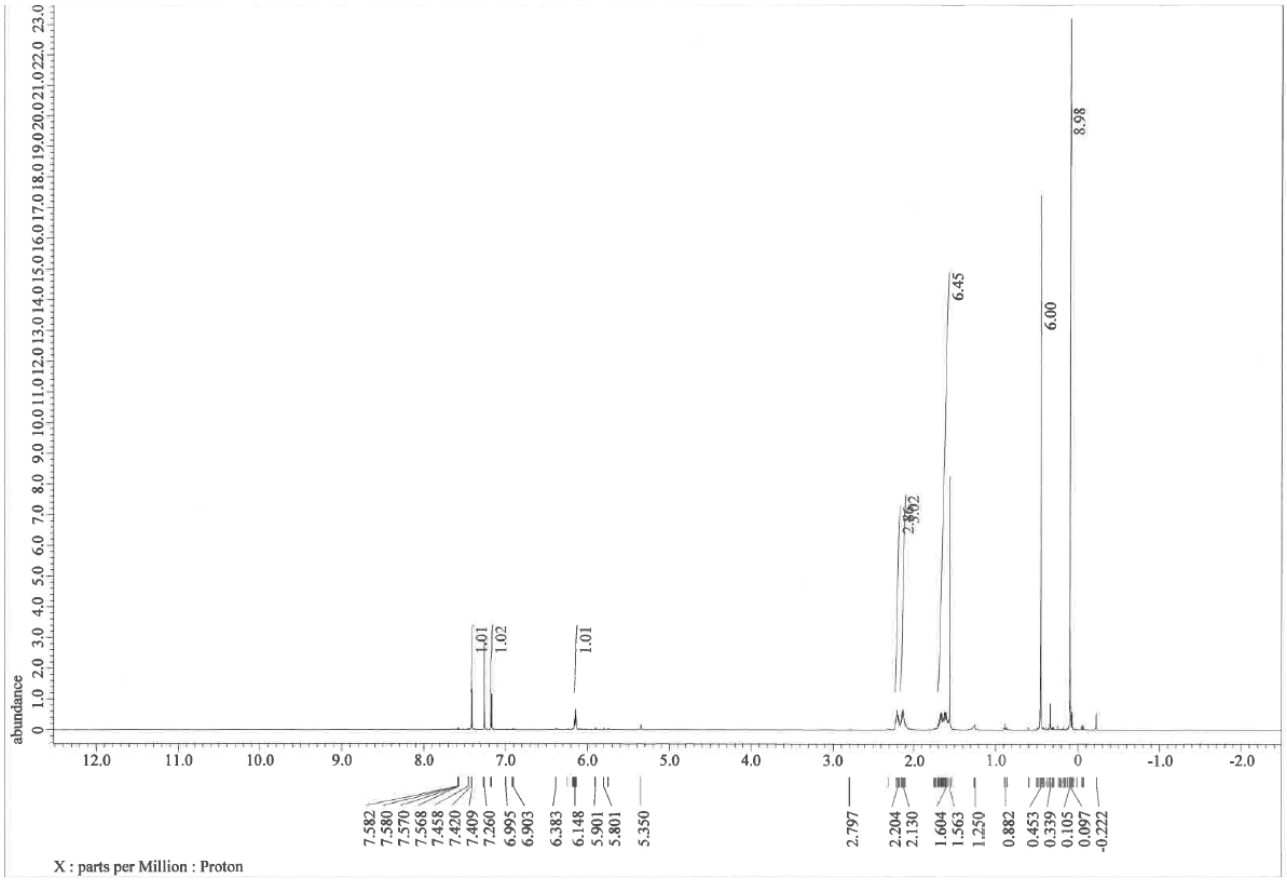

Figure S38. ^{1}H NMR spectrum of **6** in $CDCl_3$.

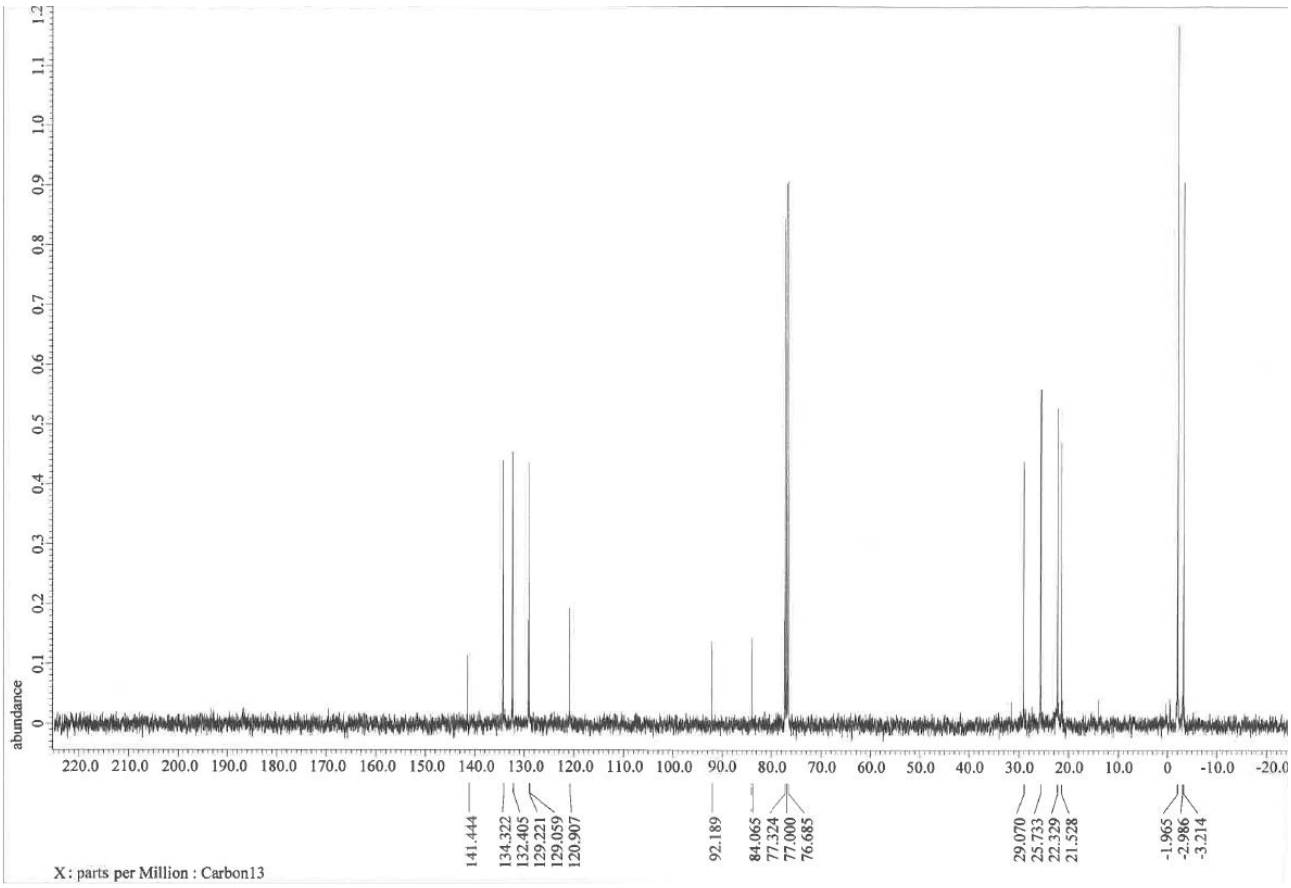

Figure S39. ^{13}C NMR spectrum of **6** in $CDCl_3$.

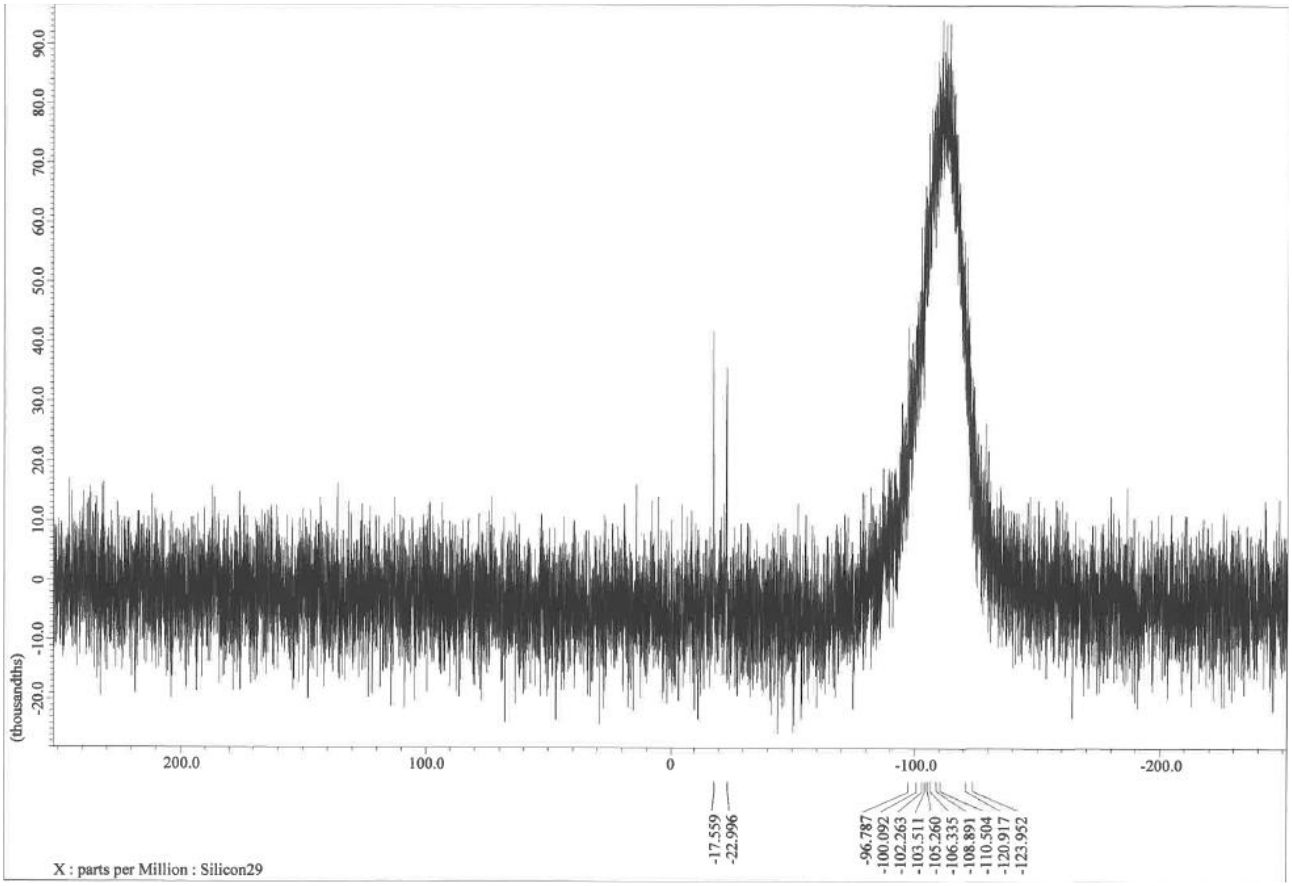

Figure S40. ^{29}Si NMR spectrum of **6** in $CDCl_3$.

Catalyst: Rh(nbd)Cl

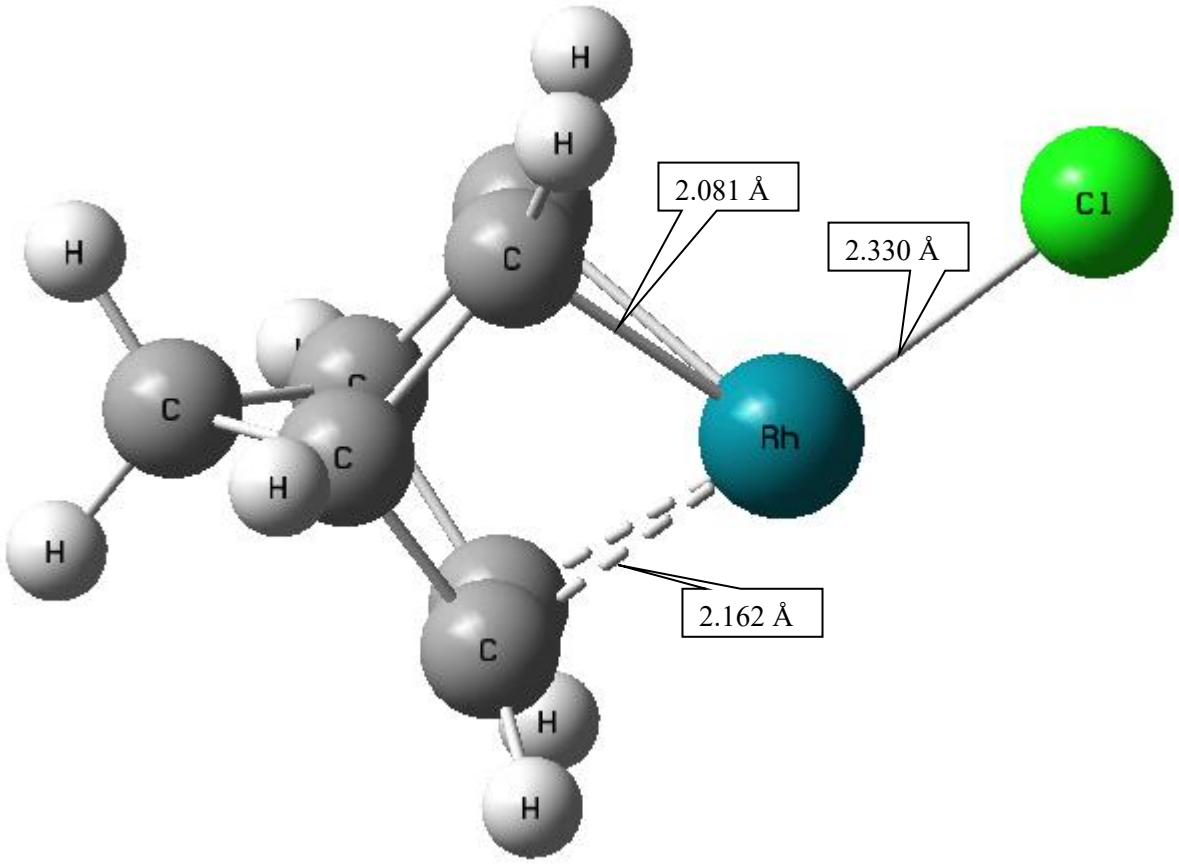

E(SCF) = -841.2814 au, E(Free) = -841.1966 au.

Figure S41. Optimized structures for RhCl(nbd) with 6-31+G(d,p) and LanL2DZ(f) basis.

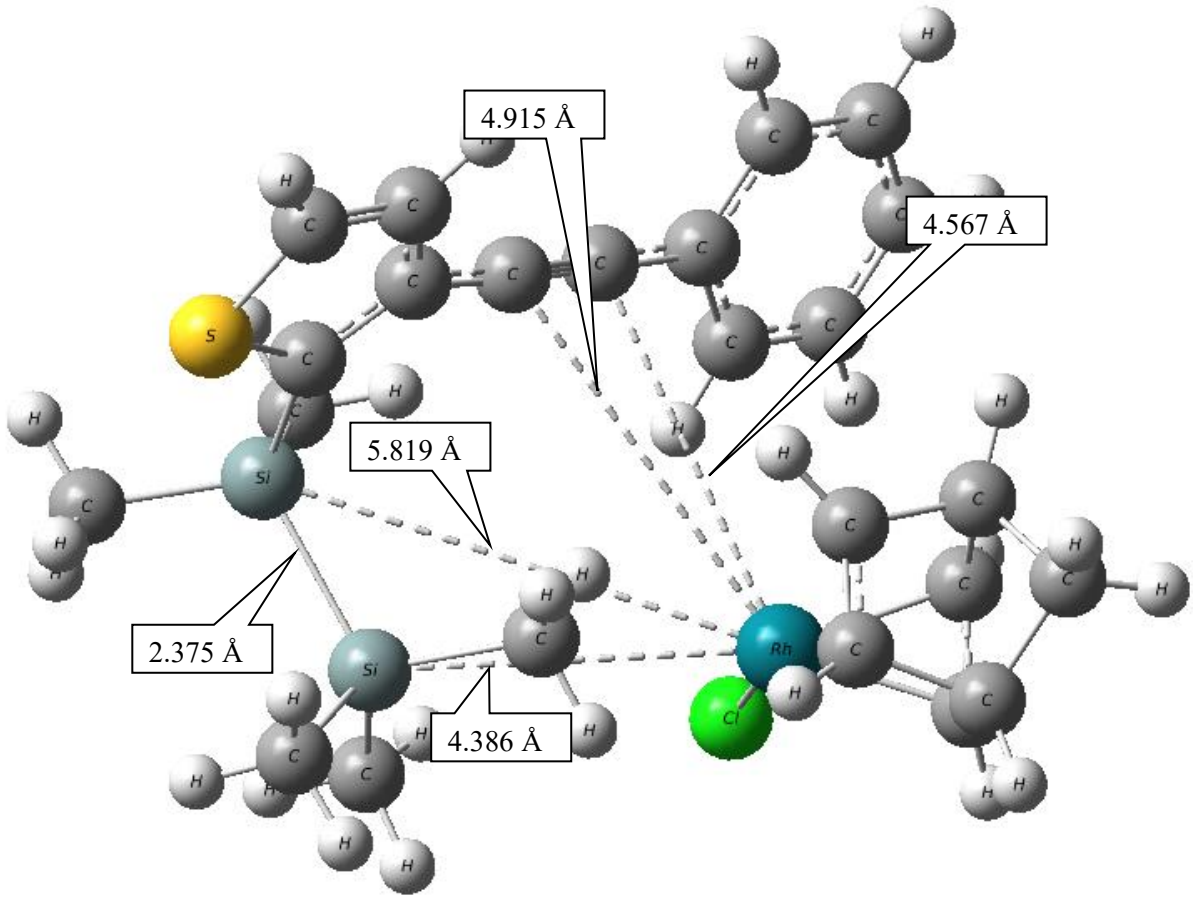

1+RhCl(nbd)
E(SCF) = -2479.5789 au, E(Free) = -2479.2160 au.

Figure S42. Optimized structure for **1** + RhCl(nbd) with 6-31+G(d,p) and LanL2DZ(f) basis.

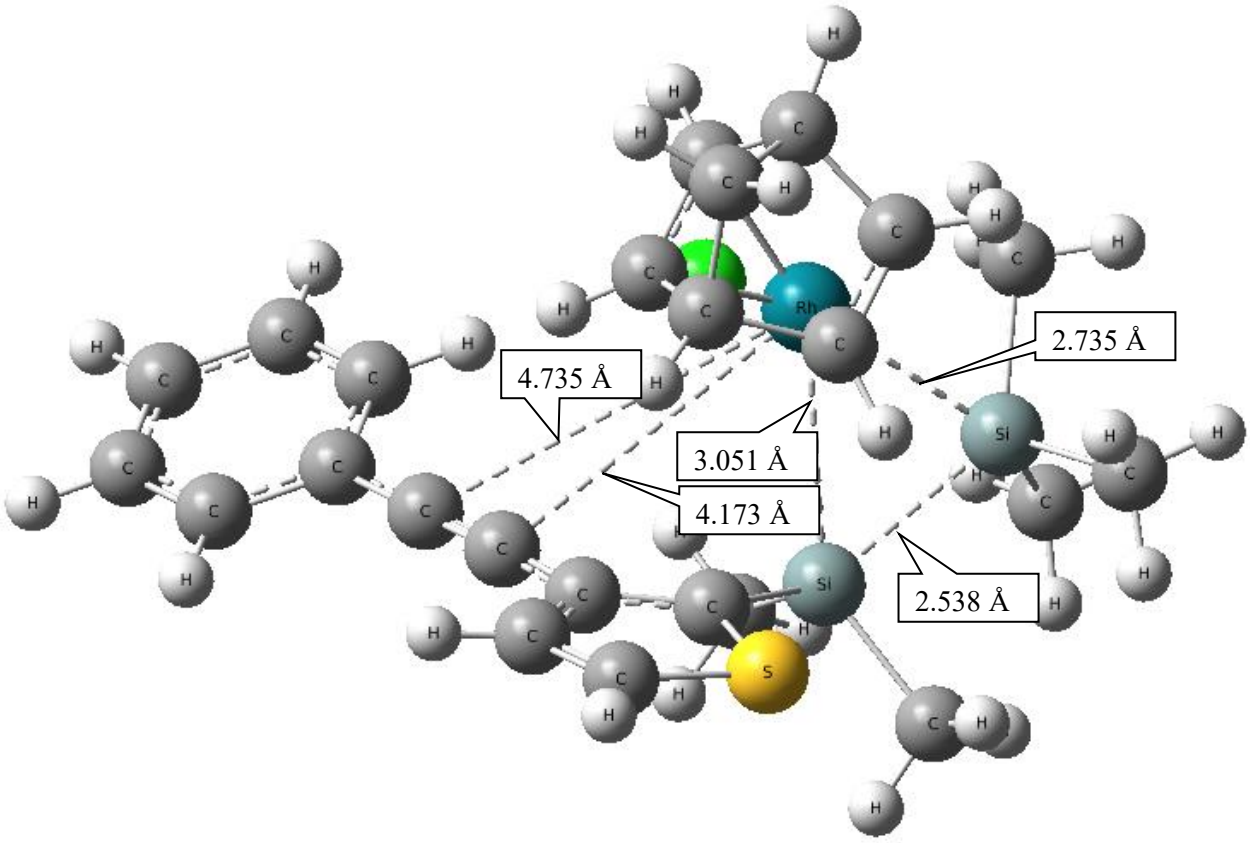

TS-0
E(SCF) = -2479.5518 au, E(Free) = -2479.1790 au.

Figure S43. Optimized structure for **TS-0** with 6-31+G(d,p) and LanL2DZ(f) basis.

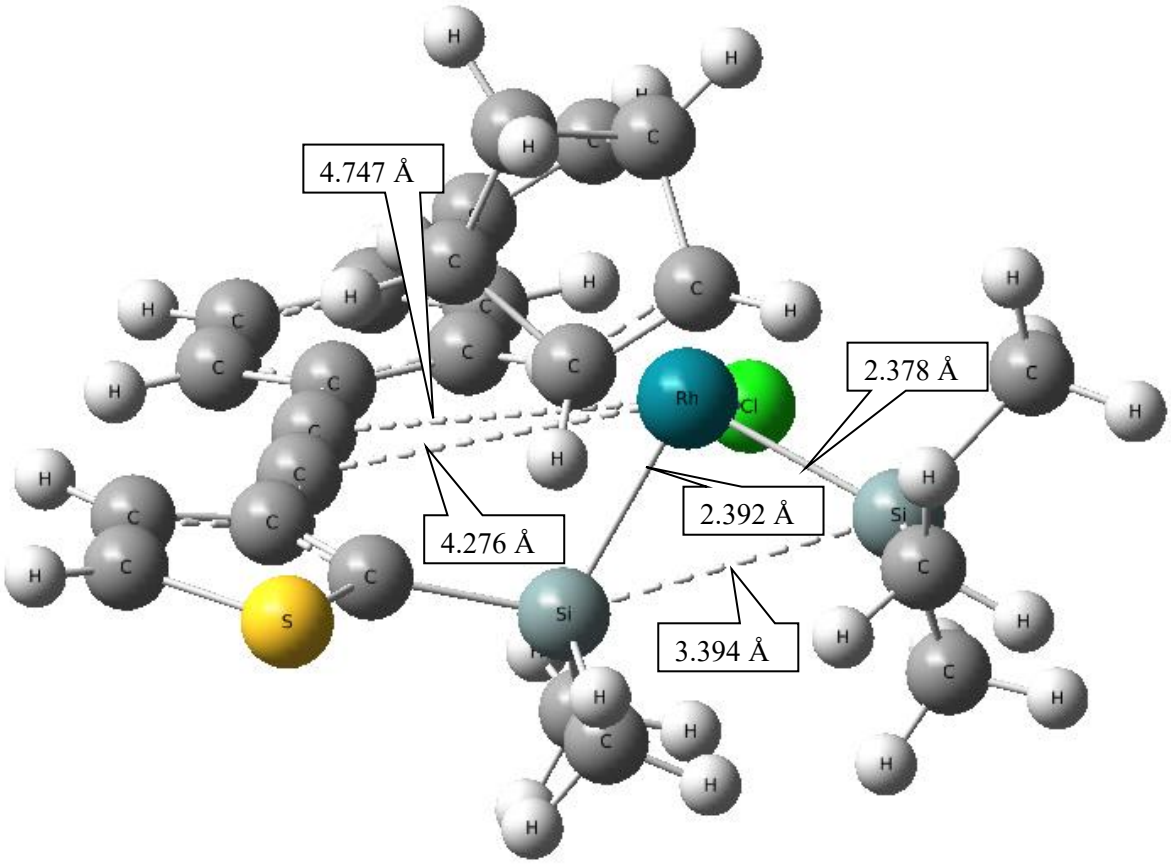

IM-1
E(SCF) = -2479.5861 au, E(Free) = -2479.2143 au.

Figure S44. Optimized structure for **IM-1** with 6-31+G(d,p) and LanL2DZ(f) basis.

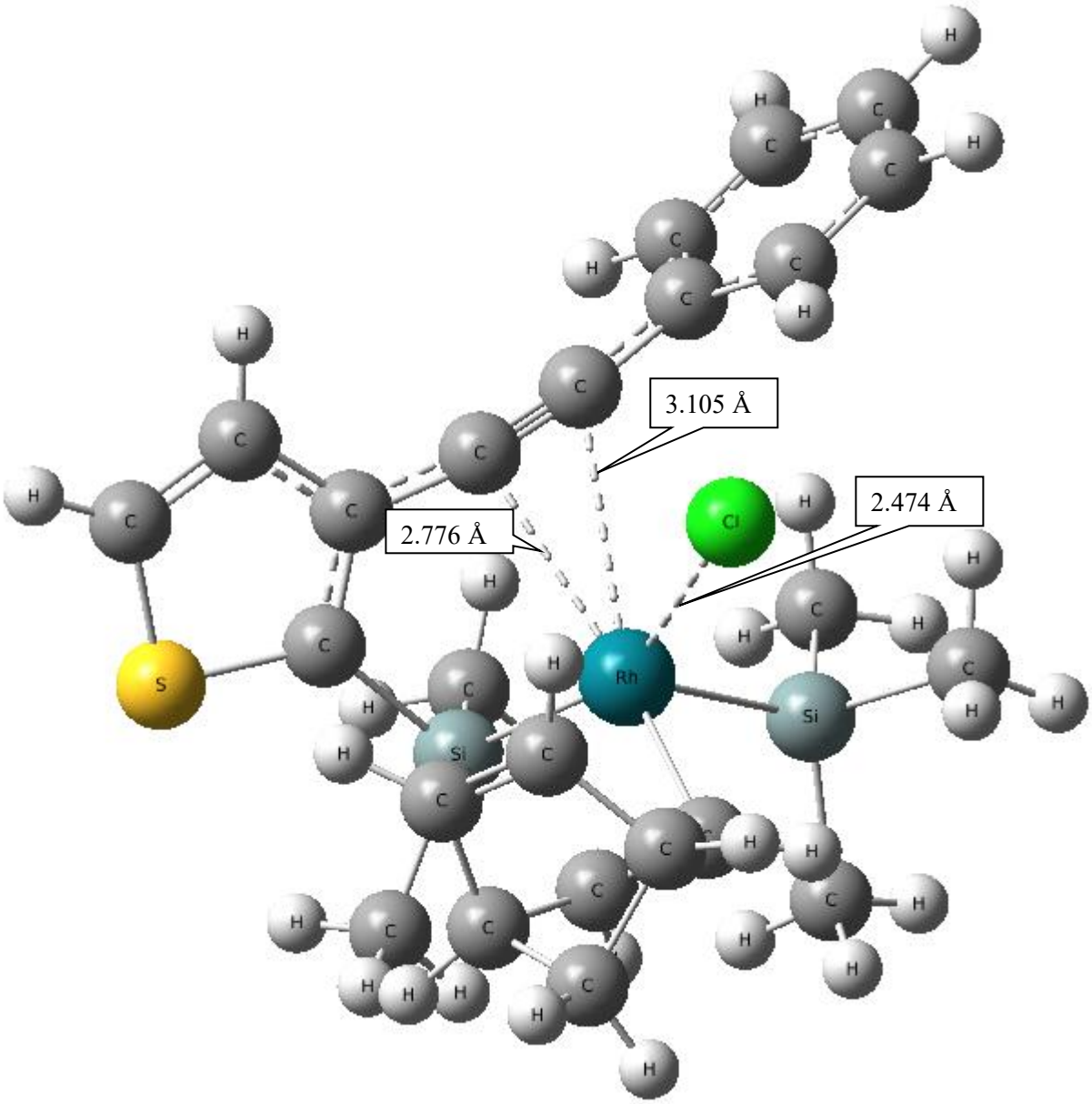

TS-1
E(SCF) = -2479.5525 au, E(Free) = -2479.1809 au.

Figure S45. Optimized structure for **TS-1** with 6-31+G(d,p) and LanL2DZ(f) basis.

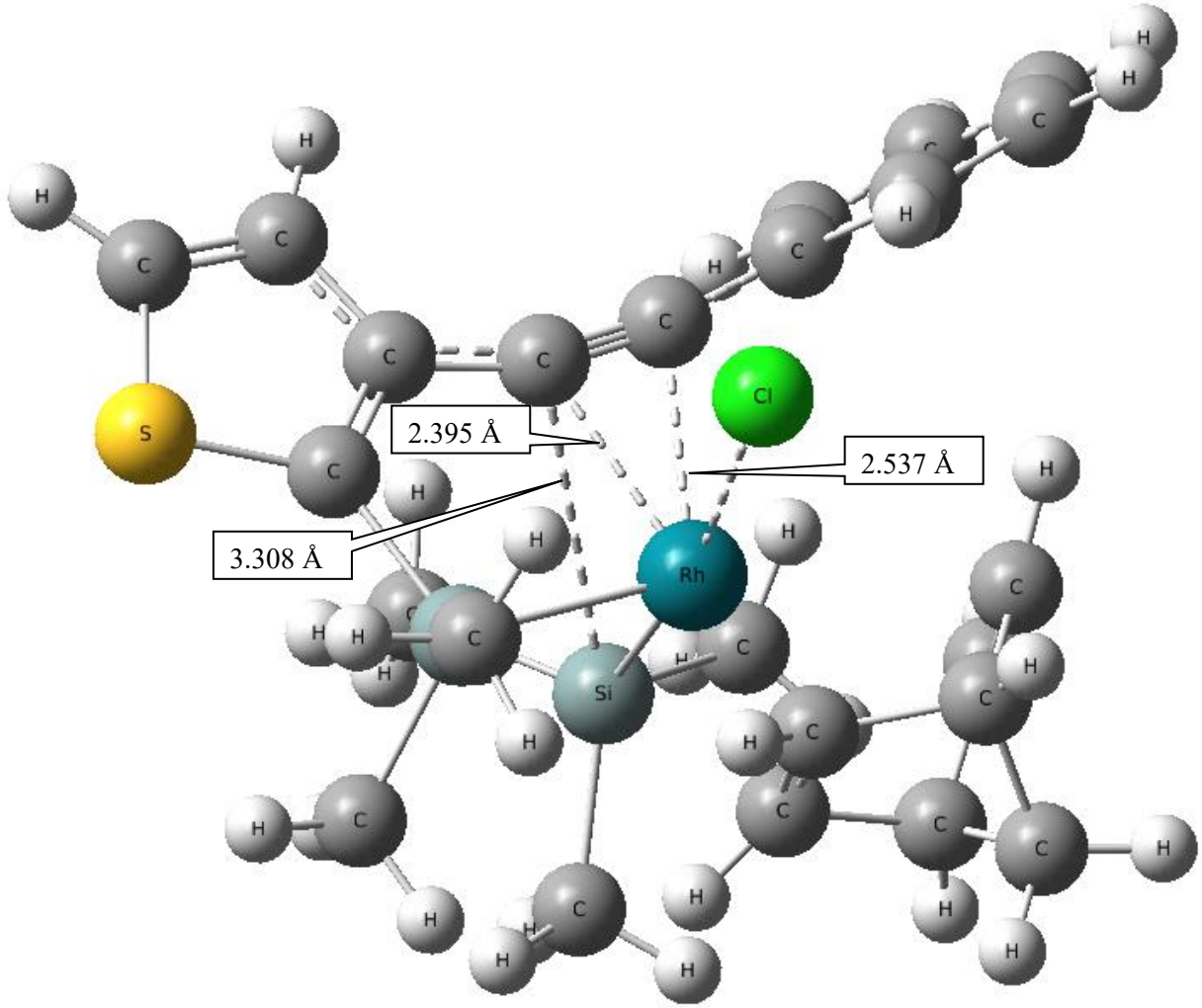

IM-2
E(SCF) = -2479.5642 au, E(Free) = -2479.1888 au.

Figure S46. Optimized structure for **IM-2** with 6-31+G(d,p) and LanL2DZ(f) basis.

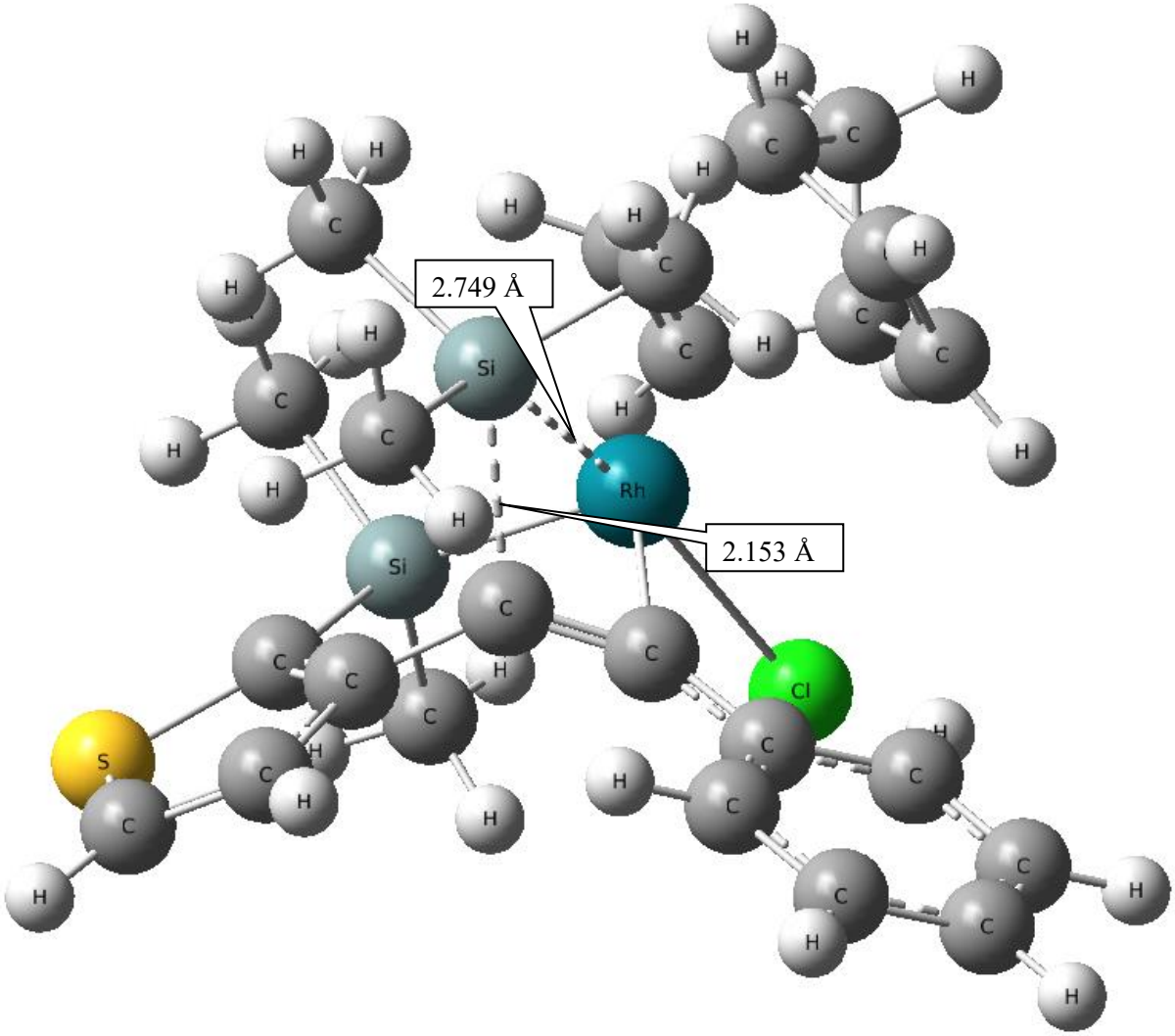

TS-2
E(SCF) = -2479.5256 au, E(Free) = -2479.1490 au.

Figure S47. Optimized structure for **TS-2** with 6-31+G(d,p) and LanL2DZ(f) basis.

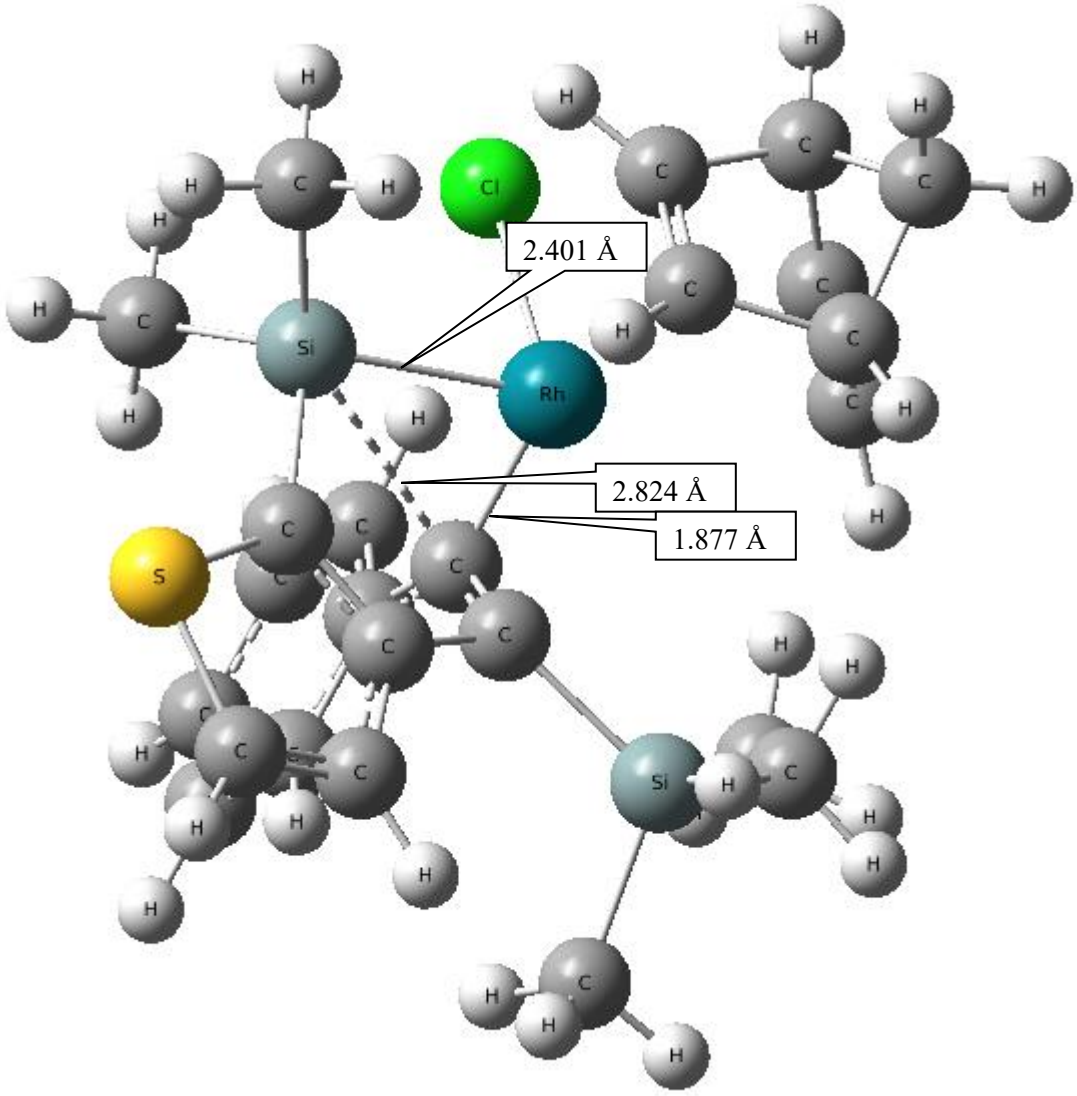

IM-3
E(SCF) = -2479.5752 au, E(Free) = -2479.2034 au.

Figure S48. Optimized structure for **IM-3** with 6-31+G(d,p) and LanL2DZ(f) basis.

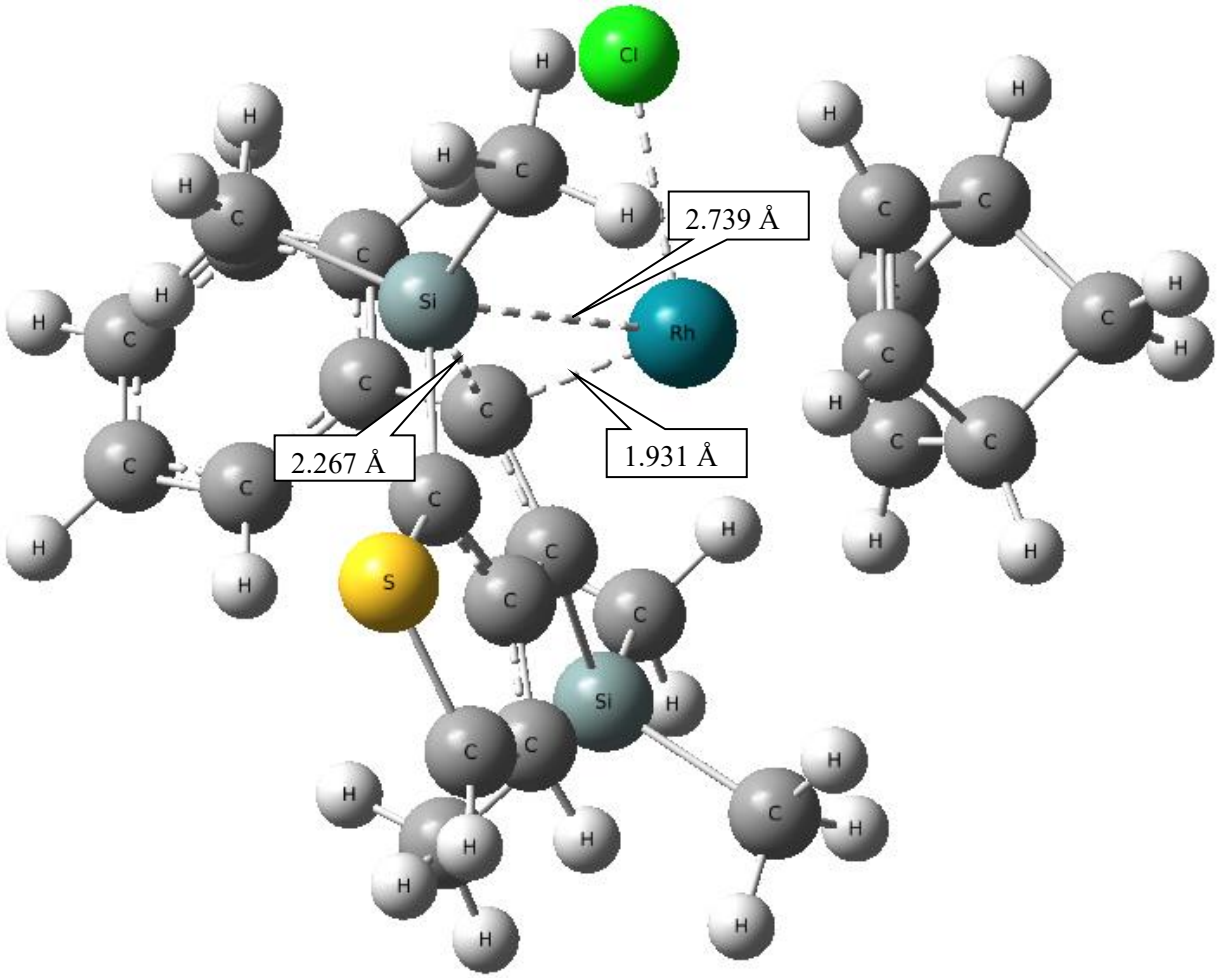

TS-3
E(SCF) = -2479.5610 au, E(Free) = -2479.1852 au

Figure S49. Optimized structure for **TS-3** with 6-31+G(d,p) and LanL2DZ(f) basis.

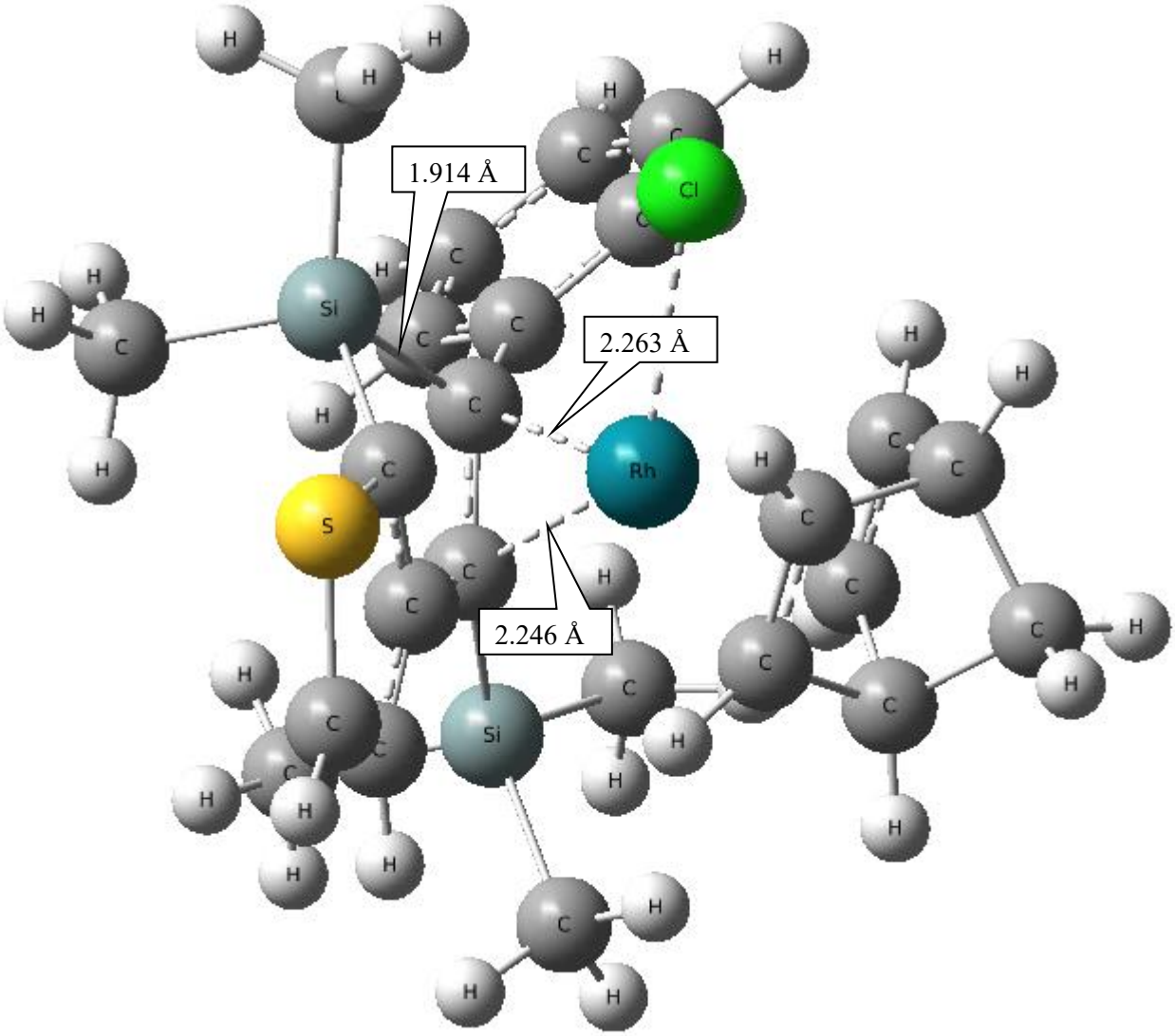

2+RhCl(nbd)
E(SCF) = -2479.6024 au, E(Free) = -2479.2270 au

Figure S50. Optimized structure for **2** + RhCl(nbd) with 6-31+G(d,p) and LanL2DZ(f) basis.